https://doi.org/10.5194/egusphere-2026-3599
Preprint. Discussion started: 26 June 2026

A Geometric Framework for Mapping Ocean Eddies Using Elliptical Streamfunction Parameterisation

Reg W. Dowse[1,3], Shane R. Keating[1,3], and Moninya Roughan[2,3]

[1]School of Mathematics and Statistics, University of New South Wales, Sydney, NSW 2052, Australia
[2]School of Biological, Earth, and Environmental Sciences, University of New South Wales, Sydney, NSW 2052, Australia
[3]Center for Marine Science and Innovation, University of New South Wales, Sydney, NSW 2052, Australia

Correspondence: Reg W. Dowse (regdowse@gmail.com)

Abstract. The identification, tracking, and characterisation of ocean eddies using observational and numerical data is essential for understanding eddy dynamics and their global climate impacts. Eulerian (point-based) and Lagrangian (trajectory-based) schemes are widely used to detect and track ocean eddies. However, these methods typically do not provide information about the spatial structure of eddies or properties such as vorticity, deformation, and vertical tilt, especially when using sparse data. Here, we describe a new efficient and robust geometrical approach for mapping the three dimensional structure of ocean eddies by fitting (partial) velocity data to a simplified elliptical streamfunction model with a small number of parameters. The flexibility of the approach is demonstrated through three variants of the method adapted to different velocity sampling patterns: single and double sections (from ship transects or a numerical grid) and scattered data (e.g. from surface drifters). We validate and demonstrate these new geometric methods on idealised, axisymmetric and non-axisymmetric Gaussian eddies, as well as numerical and observational datasets. We conclude that elliptical streamfunction parametrisation offers a versatile and effective method for research into ocean eddy characteristics.

1 Introduction

Ocean eddies are a fundamental component of ocean circulation, mediating the exchange of heat, momentum, and biogeochemical tracers, and modulating large-scale climate variability and regional processes (Wiebe and Weaver, 1999; Chelton et al., 2007; McWilliams, 2008; Gnanadesikan et al., 2013; Li et al., 2024; Roughan et al., 2017). Mesoscale eddies, with diameters of 30–300 km and lifetimes from weeks to years, play a central role in water mass transformation, nutrient transport, and biological productivity (Falkowski et al., 1991; McGillicuddy et al., 1998; McNeil et al., 1999; Benitez-Nelson et al., 2007). They are also energetically dominant features of the ocean, containing a substantial fraction of the ocean's kinetic energy and actively shaping large-scale circulation and energy pathways (McWilliams, 2008; Garabato, 2012; Klein et al., 2019). Through their coherent, rotating structures, eddies facilitate both lateral and vertical transport processes, linking large-scale circulation with smaller-scale dynamics and enhancing mixing, ventilation, and tracer redistribution throughout the ocean interior (McWilliams, 2008; Mahadevan, 2016; Renault et al., 2021).

Because of their importance, a range of techniques have been developed to detect and track mesoscale eddies using in situ

https://doi.org/10.5194/egusphere-2026-3599
Preprint. Discussion started: 26 June 2026

and remote sensing observations (e.g., Isern-Fontanet et al., 2003; Chelton et al., 2011; Nencioli et al., 2010; Vu et al., 2018). However, relatively few techniques are capable of reconstructing the evolving three-dimensional structure of mesoscale eddies, or quantifying geometric and dynamical attributes, such as vorticity, deformation, or vertical tilt, particularly when data are sparse or irregularly distributed. Eddy detection methods can be loosely organized into two categories: physical and geometric (Nencioli et al., 2010). Physical approaches, which are defined in terms of criteria for water mass properties (e.g. temperature, density, sea level anomaly) or kinematic properties (e.g. strain, vorticity), are evaluated locally. Examples include the Okubo–Weiss parameter (Okubo, 1970; Weiss, 1991; Chelton et al., 2007), sea surface height anomalies (Chelton et al., 2011), and vorticity thresholds (Mcwilliams, 1990). Although effective in dense, gridded fields, these methods depend on empirically chosen criteria and are sensitive to threshold selection, spatial resolution, and noise, often missing weak or diffuse vortices (Basdevant and Philipovitch, 1994; Sadarjoen and Post, 2000).

Geometric methods exploit the spatial organisation of the velocity field rather than its gradients. This line of investigation stems from the working definition, proposed by Robinson (1991), of a vortex as a flow feature characterized by roughly circular or spiralling instantaneous streamlines when viewed in a frame co-moving with the center of the vortex. Sadarjoen and Post (2000) adopted this definition in a method for eddy detection by evaluating the cumulative rotation of velocity vectors along gridded streamlines via the winding angle, an approach modified by Chaigneau et al. (2008) to track eddies in the South Pacific using satellite data. An alternative vector geometry-based approach proposed by Nencioli et al. (2010) identifies eddies by detecting sign reversals in gridded velocity fields. This robust and simple methodology has been widely used to identify and track vortices in gridded satellite data, numerical model output, and high-frequency radar data (Schaeffer et al., 2017; Cetina-Heredia et al., 2019; Hsu et al., 2020; Payandeh et al., 2023; Jin et al., 2024).

Similarly, spiralling and looping trajectories of Lagrangian particles — though they do not exactly match streamlines in time-evolving flows — have been used to identify vortices from global drifter datasets (Richardson, 1993; Veneziani et al., 2005a, b; Griffa et al., 2008). Brassington (2010) developed a conceptually related approach that maps surface drifter trajectories to the boundary of a time-evolving ellipse to estimate eddy velocity, vorticity, and surface divergence. Lilly et al. (2011); Lilly and Pérez-Brunius (2021) used wavelet ridge analysis to extract eddy properties by representing drifter trajectories as particle orbits around a time-varying ellipse, a method applied in the EAC by Matisons et al. (2025).

Geometrical eddy detection methods have also been adapted for use with sparse velocity measurements obtained from shipboard acoustic Doppler current profiler (S-ADCP) data. Nencioli et al. (2008) proposed a method to detect eddies using two intersecting transects within an eddy and identifying the eddy center as the point about which the mean tangential velocity attains its maximum. Luce and Rossby (2008) used an axisymmetric Gaussian streamfunction model to fit to S-ADCP velocity observations, where the fitted parameters (vortex strength and characteristic radius) provided quantitative estimates of eddy radius, amplitude, and location. More recently, Roughan et al. (2017) proposed a simple and practical geometric approach to characterise the 3D structure of two cyclonic eddies from individual S-ADCP transects. The Method of Closest Approach

https://doi.org/10.5194/egusphere-2026-3599
Preprint. Discussion started: 26 June 2026

(MOCA) locates eddy centers by tracking where the across-track velocity changes sign. Under the assumption of axisymmetric, solid-body rotation (a reasonable assumption near the inner core of an eddy), Roughan et al. (2017) were able to estimate the eddy center position and eddy vorticity. Moreover, by applying MOCA separately to each depth-bin of S-ADCP data through the watercolumn, Roughan et al. (2017) quantified the lateral displacement of the eddy center with increasing depth, thereby estimating the 'tilt' of the eddy, which impacts nutrient uplift and carbon export (Roughan et al., 2017; Belkin et al., 2020; Yang et al., 2020; Li et al., 2022a, b, 2023).

Existing geometric methods for vortex detection and characterisation have been developed in the context of specific sampling patterns of the underlying flow field, limited (of necessity) by the available observational or numerical data to gridded fields, transects, or particle trajectories. This makes it challenging to cross-validate eddy properties using independent observations, or to form a comprehensive map of eddies from multi-platform observing campaigns combining satellite, ship-based, and drifter velocity measurements. Moreover, the assumption of circular symmetry limits the accuracy of geometrical methods in elliptical or distorted flows — properties that are essential for describing realistic, non-axisymmetric vortices.

In this study, we seek to address these limitations by developing a flexible geometric method for mapping and tracking ocean eddies that is suitable for any sampling pattern of the flow field, including gridded velocity fields (Cartesian or curvilinear), velocity transects (through the water column), or surface velocities estimated from Lagrangian drifter trajectories. The method generalises existing geometric frameworks through an Elliptical Streamfunction Parametrisation (ESP), which assumes that velocity vectors are tangent to elliptical streamlines centered on the eddy core. This approach provides a compact, physically interpretable representation of both circular and elliptical vortices that is adaptable to any sampling pattern of the underlying flow field.

Here we present a new simple and robust algorithm for retrieving the ESP properties for a given eddy — including center position, deformation, vorticity, radius, amplitude and tilt — from partial or irregular velocity observations. To emphasize the speed and versatility of the approach, we call this the ESPresso method. The ESPresso method is a threshold-free, data-efficient framework that unifies previous geometric methods into a single model capable of mapping realistic eddy structure and evolution. We further present three variants of the ESPresso method that are adapted to specific sampling patterns: SOLO (for single transects, e.g. ship tracks), DOPPIO (for double orthogonal transects, e.g. gridded or satellite data), and LATTE (for Lagrangian trajectories and other unstructured velocity data, e.g. from ocean drifters). In each case, we discuss the potential biases (and their remedies) arising from particular sampling patterns. We conclude with a case study that applies the ESPresso method to data from a multiplatform field campaign combining in-situ, satellite, and drifter observations of velocities in a large mesoscale cyclonic eddy.

Beyond instantaneous mapping, the ESPresso framework naturally extends to both temporal and vertical analyses. When applied sequentially in time, it enables tracking of eddy evolution and propagation while reconstructing the full velocity field

https://doi.org/10.5194/egusphere-2026-3599
Preprint. Discussion started: 26 June 2026

at each time step. The same approach can be applied across depth levels to recover the vertical structure of the velocity field from partial observations. When combined in both time and depth, this enables reconstruction of the time-evolving three-dimensional velocity field of the eddy, providing a pathway to quantify depth-dependent properties such as vertical tilt and the dynamical evolution of eddy structure.

This paper is organised as follows. Section 2 outlines the Elliptical Streamfunction Parameterisation (ESP) model and the ESPresso method for determining the model parameters from sparse velocity data, and describes the model and observational data sets used to validate the methods. Section 3 describes three variants of the ESPresso method adapted for common velocity sampling patterns (SOLO, DOPPIO, LATTE) and analyses the performance of the methods tested with idealised eddy velocity fields, numerical model output, and observational data. Section 4 provides conclusions.

2 Methods and Data

2.1 Elliptical Streamfunction Parametrisation

The Elliptical Streamfunction Parametrisation (ESP) framework assumes that streamlines form closed ellipses centered on the eddy core. Under this formulation, sparse velocity measurements within the eddy field are used to infer key flow characteristics, including the eddy center, vorticity, deformation, size, scale, and tilt (when applied through the water column). In the ESP approximation, the streamfunction $\psi(\rho)$ is expressed as a function of the effective radius

$$\rho(x,y) = \| \, (\boldsymbol{x} - \boldsymbol{x_0})^\intercal \, Q \, (\boldsymbol{x} - \boldsymbol{x_0}) \, \|^{1/2}, \tag{1}$$

where $\boldsymbol{x_0} = (x_0, y_0)^\intercal$ denotes the eddy center and Q is a real, symmetric, non-negative matrix describing the vortex geometry,

$$Q = \begin{bmatrix} q_{11} & q_{12} \\ q_{12} & q_{22} \end{bmatrix}, \qquad \det(Q) = 1, \qquad q_{11}, q_{22} > 0, \tag{2}$$

The matrix Q has real, positive eigenvalues λ and λ^{-1} (where $\lambda \geq 1$) with eigenvectors $\boldsymbol{v}^{\pm}$ defining the principal axes of an ellipse with semimajor axis $a = \lambda^{1/2}\rho$, semiminor axis $b = \lambda^{-1/2}\rho$, and aspect ratio $\alpha = a/b = \lambda$. The effective radius ρ can therefore be interpreted as the radius of a circle with area $\pi\rho^2 = \pi ab$ equal to that bounded by the ellipse $\rho(x,y) = \text{constant}$.

Following Luce and Rossby (2008), we model the streamfunction with a non-axisymmetric Gaussian profile with amplitude ψ_0 and characteristic radius R_c,

$$\psi(\rho) = \psi_0 \exp\left(-\frac{\rho^2}{R_c^2}\right). \tag{3}$$

This form represents a divergence-free horizontal velocity field $\boldsymbol{u} = \boldsymbol{\nabla}^\perp \psi = (-\psi_y, \psi_x)^\intercal$ with vorticity $\omega = \hat{\boldsymbol{z}} \cdot (\nabla \times \boldsymbol{u}) = \nabla^2 \psi$. Within the inner core, $\psi(\rho)$ can be approximated as a quadratic function of the effective radius, $\psi^{\text{core}} \approx \psi_0 \left(1 - \rho^2/R_c^2\right)$, and

https://doi.org/10.5194/egusphere-2026-3599
Preprint. Discussion started: 26 June 2026

the velocity field becomes

$$u^{\text{core}} = -\psi_y^{\text{core}} = \frac{2\psi_0}{R_c^2}\left(q_{12}(x-x_0) + q_{22}(y-y_0)\right) \tag{4}$$

$$v^{\text{core}} = \psi_x^{\text{core}} = -\frac{2\psi_0}{R_c^2}\left(q_{11}(x-x_0) + q_{12}(y-y_0)\right). \tag{5}$$

This can be compactly written as

$$\boldsymbol{u}^{\text{core}} = \Omega\, JQ\,(\boldsymbol{x}-\boldsymbol{x_0}), \quad \text{where} \quad J = \begin{bmatrix} 0 & -1 \\ 1 & 0 \end{bmatrix}, \tag{6}$$

and $\Omega = -2\psi_0/R_c^2$. The vorticity of the flow is

$$\omega^{\text{core}} = \Omega\ (q_{11}+q_{22}) = 2\Omega\left(\frac{\alpha+\alpha^{-1}}{2}\right). \tag{7}$$

Thus, sufficiently close to the eddy inner core, the velocity field has uniform vorticity ω^{core} determined by Ω and the aspect ratio α. For a circular eddy ($Q = I$, $\alpha = 1$), the inner core is in solid body rotation (Rossby et al., 2011; Rossby, 2014; Belkin et al., 2020) with angular velocity Ω and vorticity $\omega^{\text{core}} = 2\Omega$. More generally, the flow around the core will have a slower tangential velocity near the long axis of the ellipse and a faster tangential velocity near the short axis. Away from the inner core, the outer core of the eddy has velocity, tangential velocity and vorticity given by

$$\boldsymbol{u} = \boldsymbol{u}^{\text{core}}\, e^{-\rho^2/R_c^2}, \qquad \omega = \omega^{\text{core}}\, e^{-\rho^2/R_c^2}. \tag{8}$$

2.2 Estimation of Elliptical Streamfunction Parameters from velocity data

In the ESPresso method, the eddy center $\boldsymbol{x_0}$, vortex geometry Q and angular velocity Ω are first estimated by fitting the inner-core flow field to spatially distributed velocity data measured sufficiently close to the eddy center. The streamfunction amplitude ψ_0 and characteristic radius R_c are subsequently estimated by including measurements from the outer core of the eddy. The transition from 'inner-core' to 'outer-core' velocity data can be checked a posteriori using goodness-of-fit of the inner-core data to a uniform vorticity flow; if needed, the population of inner-core sample points can be adjusted by changing the search radius around the initial guess for the eddy center.

Given observed velocities $\hat{\boldsymbol{u}}_i = (\hat{u}_i, \hat{v}_i)^T$ at points $\hat{\boldsymbol{x}}_i = (\hat{x}_i, \hat{y}_i)^T$ within the eddy inner core, the ESPresso method finds parameters x_0, y_0, Ω, and Q that minimize the sum of squared residuals

$$\mathcal{R}^{\text{core}} = \sum_i \left|\hat{\boldsymbol{u}}_i - \boldsymbol{u}^{\text{core}}\left(\hat{\boldsymbol{x}}_i; \boldsymbol{x_0}, \Omega, Q\right)\right|^2. \tag{9}$$

From Q, it is straightforward to calculate the principle axes $\boldsymbol{v}^{\pm}$ and aspect ratio α of the inner core. The most suitable procedure for minimizing (9) depends on the spatial distribution of the sampling pattern, resulting in variants of the ESPresso method for single transect velocity observations (SOLO), double orthogonal transect velocity observations (DOPPIO), and Lagrangian,

https://doi.org/10.5194/egusphere-2026-3599
Preprint. Discussion started: 26 June 2026

unstructured or multi-platform velocity observations (LATTE). These variants are described in detail in Section 3.

Once the inner-core parameters have been determined, the characteristic radius R_c and eddy amplitude ψ_0 are estimated using velocity data from both the inner and outer core. At each measurement point $\hat{\boldsymbol{x}}_i$, we calculate the tangential velocity by projecting the velocity data $\hat{\boldsymbol{u}}_i$ along the tangential direction,

$$\hat{V}_{T,i} = \boldsymbol{t}(\hat{\boldsymbol{x}}_i) \cdot \hat{\boldsymbol{u}}_i, \quad \text{where} \quad \boldsymbol{t}(\hat{\boldsymbol{x}}_i) = \frac{JQ(\hat{\boldsymbol{x}}_i - \boldsymbol{x_0})}{\|Q(\hat{\boldsymbol{x}}_i - \boldsymbol{x_0})\|} \tag{10}$$

is the unit tangent to the ellipse at the measurement point $\hat{\boldsymbol{x}}_i$. For elliptical eddies, the tangential velocity along a given streamline will vary with azimuthal angle, being maximum near the short axis and minimum near the long axis of the ellipse. To compare velocity data with different azimuthal angles around the ellipse, we calculate the *normalized tangential velocity* as

$$\hat{V}^{\star}_{T,i} = \hat{V}_{T,i} \frac{\rho(\hat{\boldsymbol{x}}_i)}{\|Q(\hat{\boldsymbol{x}}_i - \boldsymbol{x_0})\|}. \tag{11}$$

This normalisation removes the geometric dependence introduced by Q, such that the tangential velocity profile of the elliptical streamfunction parametrisation is independent of the azimuthal angle. To see this, we calculate the modelled tangential velocity using the elliptical streamfunction parametrisation

$$V^{\star}_T(\rho) = \frac{\rho\, \boldsymbol{t}(\boldsymbol{x}) \cdot \boldsymbol{u}(\boldsymbol{x})}{\|Q(\boldsymbol{x} - \boldsymbol{x_0})\|} = \Omega \rho\, e^{-\rho^2/R_c^2}. \tag{12}$$

Thus, in all azimuthal directions, the normalized tangential velocity $V^{\star}_T(\rho)$ has a Gaussian profile peaked at effective radius $\rho = R_c/\sqrt{2}$.

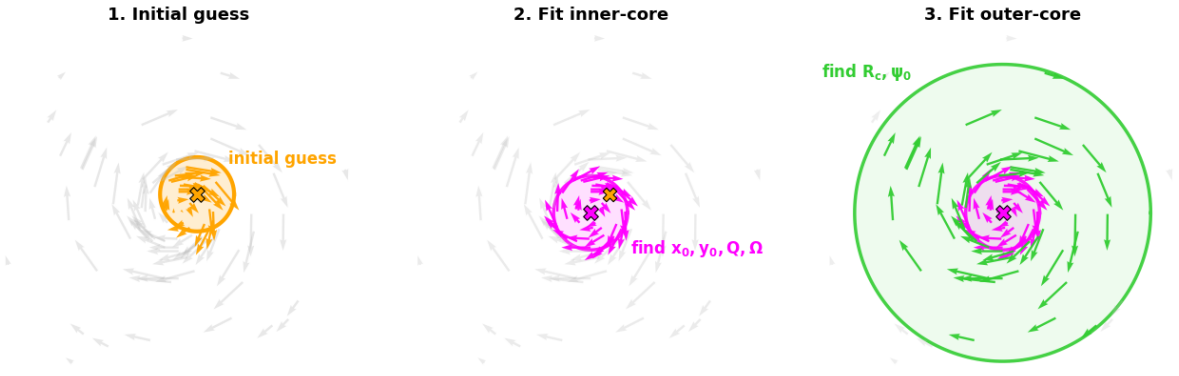

Figure 1. Schematic of the ESPresso procedure. (1) An initial estimate of inner-core data is obtained. (2) The data identified in (1) are used to estimate the inner-core parameters, identifying the eddy center. (3) The inner-core parameters (x_0, y_0, Q, Ω) define ρ, which is used to select outer-core data and estimate (R_c, ψ_0).

https://doi.org/10.5194/egusphere-2026-3599
Preprint. Discussion started: 26 June 2026

The parameters Ω (refined) and R_c are estimated by minimising the sum of squared residuals between the measured tangential velocity data (11) and the tangential velocity of the ESP modelled eddy at each measurement point (12),

$$\mathcal{R}^{\text{outer}} = \sum_i \left| \hat{V}^{\star}_{T,i} - V^{\star}_T \left(\hat{\boldsymbol{x}}_{\boldsymbol{i}}; \Omega, R_c \right) \right|^2 . \tag{13}$$

Optimisation in this study is performed using the `curve_fit` function from the `SciPy` Python package (v1.15.3), which employs non-linear least squares minimization of $\mathcal{R}^{\text{outer}}$ over the parameters (Ω, R_c). The initial guess for Ω is taken from the value obtained from the $\mathcal{R}^{\text{core}}$ minimisation. The initial guess for R_c is set to R_{max}, where $R_{\text{max}} = \sqrt{2}\rho_{\text{max}}$ and ρ_{max} is the radial distance at which the maximum (normalised) tangential velocity is observed.

During the minimisation of $\mathcal{R}^{\text{outer}}$, Ω is treated as a free parameter to improve the stability of the optimisation for R_c. This procedure yields a refined estimate of Ω, which is adopted as the final value and used to update the inner-core vorticity ω. The amplitude is then computed as $\psi_0 = -\Omega R_c^2/2$.

The ESPresso framework (illustrated in Figure 1) can be applied to sequences of velocity data in both time and depth. At each time step or depth level, the ESP parameters are estimated, and the analysis is advanced by centering the subsequent computation on the previously identified eddy center. This sequential procedure enables temporal tracking of eddies and, when applied across depth levels, reconstruction of their three-dimensional structure through the water column. In this study, the temporal application is demonstrated using the DOPPIO and LATTE methods.

2.3 Model and observational datasets

All datasets were obtained in the same cyclonic eddy (CE) located off the southeast coast of Australia and include shipboard acoustic Doppler current meter (S-ADCP) measurements, satellite-derived geostrophic velocities, drifter velocity observations, and numerical hydrodynamic model output of surface velocities.

The eddy was first identified within the Tasman Sea on 19 October 2023 (UTC) and subsequently propagated westward until at least 11 February 2024. Inspection of satellite velocity fields placed the eddy center at approximately (154.3°E, 37.9°S) on 19 October 2023. A local Cartesian (X, Y) coordinate system was constructed around this point and used throughout the study.

2.3.1 S-ADCP velocity data

Near-surface (∼37 m depth) S-ADCP data were collected during a 23-day research voyage aboard the Australian Marine National Facility vessel *RV Investigator* IN2023-V06 (CSIRO Marine National Facility; http://www.csiro.au/en/Research/Facilities/Marine-National-Facility). A quasi-straight transect across the CE from 2023-10-17T13:42 to 2023-10-18T13:27 (UTC) is used in this study (Figure 6). The S-ADCP velocity data have a temporal resolution of 15 min. Full details of the cruise and associated datasets are provided in Azaneu et al. (2025).

https://doi.org/10.5194/egusphere-2026-3599
Preprint. Discussion started: 26 June 2026

In addition to this transect, the full S-ADCP dataset spanning multiple crossings of the eddy between 17 October and 2 November 2023 is also used (Figure 12), providing both quasi-linear and irregular sampling of the flow field.

2.3.2 Modelled gridded velocity fields

Gridded velocity fields were obtained from the Operational Mercator Global Ocean Analysis and Forecast System (E.U. Copernicus Marine Service Information (CMEMS), 2024). The Mercator system provides daily global ocean forecasts at a horizontal resolution of $1/12°$. For this study, a regional subset (149–158°E, 34–42°S) spanning 19 October 2023 to 27 January 2024 was extracted to capture the spatio-temporal evolution of the CE.

2.3.3 Satellite-derived velocity data

Geostrophic velocity fields derived from satellite altimetry were obtained from the Integrated Marine Observing System (IMOS) (Australian Ocean Data Network, 2026). The dataset covers the domain 149–158°E and 34–42°S at a horizontal resolution of $1/5°$. For analyses involving S-ADCP data, satellite fields were linearly interpolated to the mean S-ADCP observation time (2023-10-19T16:30), while for time-evolving analyses, daily fields spanning the CE lifetime (19 October 2023 to 27 January 2024) were used.

2.3.4 Drifter velocity data

Drifter trajectories and velocities were obtained from the NOAA Observing System Monitoring Center (OSMC; https://osmc.noaa.gov/erddap/tabledap/OSMC_flattened.html) and the Global Drifter Program (GDP). Two SVP drifters, drogued at $\sim$15 m depth to represent near-surface velocities, were deployed within the CE during the research cruise. These drifters provided velocity measurements between 19 October 2023 and 9 February 2024 at 6-hour intervals.

For combined analyses, drifter observations were temporally associated with satellite velocity fields using a ± 1 day window (Figure 13). Thus, for a given day, the dataset consists of the satellite velocity field together with all drifter observations recorded within one day before and after that timestamp.

3 Results

3.1 SOLO (Single straight-line transect)

Velocity measurements along straight lines are common in both numerical model output (e.g., along coordinate axes) and observational datasets (e.g., shipboard ADCP transects). However, such measurements alone do not uniquely constrain the ESP model, as multiple parameter combinations can reproduce the observed velocities along a single transect. Consequently, the inverse problem is underdetermined when only one-dimensional velocity data are available.

https://doi.org/10.5194/egusphere-2026-3599
Preprint. Discussion started: 26 June 2026

The Method of Closest Approach (MOCA), introduced by Roughan et al. (2017), addresses this limitation by assuming that the velocity field is modelled as uniformly rotating axisymmetric flow. Under this assumption, the velocity field is approximated as $\boldsymbol{u} = \boldsymbol{u}^{\text{core}}$, which is valid near the eddy center but degrades with distance from the inner core. Including velocity data far from the inner core can therefore introduce bias in the estimated eddy center and angular velocity. Here, we present a modification of this approach, SOLO, which mitigates this bias by restricting the fit to velocity observations near the point of closest approach.

We adopt a coordinate system that is aligned with the velocity sampling pattern: velocity measurements $(\hat{u}_i, \hat{v}_i)$ are taken along a straight line transect $(x, 0)$ passing through $y = 0$. An axisymmetric eddy is assumed to be centered at (x_0, y_0), so that the point of closest approach along the transect is $x = x_0$ and the distance of the eddy center from this point is y_0. Near the inner core, the ESP model velocities along a single straight line transect are $u^{\text{core}}(x, 0) = \Omega\,(q_{12}(x - x_0) - q_{22} y_0)$ and $v^{\text{core}}(x, 0) = -\Omega\,(q_{11}(x - x_0) - q_{12} y_0)$. This system has six unknowns $(\Omega, x_0, y_0, q_{11}, q_{22}, q_{12})$ and one constraint $(\det Q = 1)$. Thus, a linear least squares fit of the measured velocities will result in four parameters for five independent variables, and the system is underdetermined.

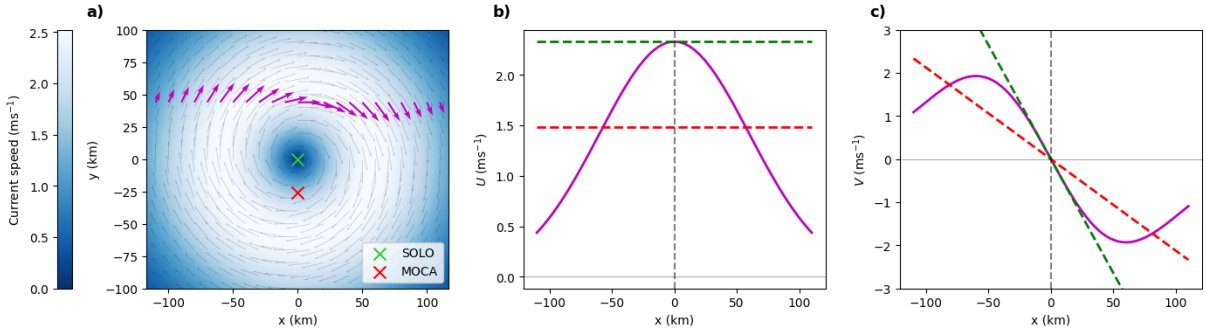

Figure 2. (a) A straight-line transect (magenta quivers) across an axisymmetric Gaussian eddy. The MOCA and SOLO methods are applied to estimate the eddy center (×). (b) Tangential velocity along the transect with the MOCA linear regression fit (red dotted line); the SOLO estimate at the point of closest approach x_0 is indicated by the green dotted line. (c) Same as (b), but for the normal velocity along the transect. The green dotted line represents the SOLO tangent fit at x_0, while the red dotted line shows the original MOCA linear fit.

Following Roughan et al. (2017), we assume an axisymmetric eddy geometry ($q_{11} = q_{22} = 1$, $q_{12} = 0$), in which case

$$u^{\text{core}}(x, 0) = \Omega y_0, \qquad v^{\text{core}}(x, 0) = \Omega(x - x_0). \tag{14}$$

The MOCA approach seeks a linear least-squares fit of the measured velocities, $\hat{u}_i = a\hat{x}_i + b$, $\hat{v}_i = c\hat{x}_i + d$ and estimates the eddy properties via the relations

$$x_0 = -\frac{d}{c}, \qquad y_0 = \frac{b}{c}, \qquad \Omega = c, \tag{15}$$

https://doi.org/10.5194/egusphere-2026-3599
Preprint. Discussion started: 26 June 2026

where a, b, c, d are the parameters of the least squares fit. Note that $a = 0$ because, by construction, the along-track velocity u^{core} does not vary in x direction under the assumption of solid body rotation.

A drawback of the MOCA method is that it tends to underestimate the angular velocity of the eddy Ω and hence overestimates the distance from the eddy center y_0. This is illustrated in Figure 2, which shows velocity measurements along a straight-line transect passing an idealized circular eddy with a Gaussian outer core. As can be seen in panel (b), the along-track velocity u is approximately constant only near the point of closest approach ($x = 0$). Away from this region, the along-track velocity decays rapidly. Likewise, the across-track velocity v, shown in panel (c), is linear only near the point of closest approach. In both cases, a least-squares fit to the data (shown in red) will underestimate the along-track velocity and the slope of the across-track velocity, resulting in an underestimate of the angular velocity $\Omega = -2.1 \times 10^{-5}$ s^{-1} compared to the true value of $\Omega = -6.9 \times 10^{-5}$ s^{-1}, and an overestimate of the distance to the eddy center $y_0 = -25.8$ km vs the true value of $y_0 = 0$ km (shown by the red $\times$ in Figure 2a).

The SOLO method corrects for this bias by limiting the data points to those nearest the point of closest approach. This is achieved by narrowing the search radius for the inner core to sample points around the location where the cross-track velocity v changes sign ($x = x_0$). The inner-core velocities, satisfying $|x - x_0| \leq 30$ km (adjustable depending on eddy size), are then fitted using even and odd polynomial forms: $U(x) = A + B(x - x_0)^2$ and $V(x) = C(x - x_0) + D(x - x_0)^3$. This allows for a better representation of the behaviour of u and v near $x = x_0$ than can be achieved by a linear fit. Specifically, close to $x = x_0$, the polynomials are approximately $U(x) \approx U(x_0)$ and $V(x) \approx V'(x_0)(x - x_0)$, from which we can derive the eddy center and angular velocity as

$$x_0 : V(x_0) = 0, \qquad y_0 = \frac{U(x_0)}{V'(x_0)}, \qquad \Omega = V'(x_0). \tag{16}$$

Intuitively, the point of closest approach x_0 represents the x-value where the across-track velocity $V(x)$ changes sign and $V'(x_0)$ is the slope of the across-track velocity at this point. This approach effectively corrects for the bias introduced by MOCA in the estimate of the angular velocity Ω and distance of closest approach y_0 (see Figure 2b, c).

3.1.1 Idealized Model Validation

Examples illustrating the SOLO method are shown in Figure 3. Transects were first positioned at different proximity from the center of an axisymmetric idealised eddy (P1: $y = 20$ km; P2: $y = 50$ km; P3: $y = 80$ km, each with transect length 70 km). A second set of tests used transects of varying lengths through the same eddy (L1: 80 km; L2: 140 km; L3: 200 km), each centered at $(x, y) = (0, 20$ km). The resulting ESP parameter estimates are summarised in Table 1.

Across all tests (P1–P3, L1–L3), the SOLO method provides robust estimates of the eddy center, rotation rate, and core radius (Table 1). Errors in the estimated eddy center remain below 3 km ($< 4\%$ of eddy core radius). The outer-core fitting, based on the normalised tangential velocity (Figure 4), shows negligible error (< 2 km, $< 3\%$ of eddy core radius) in identifying the

https://doi.org/10.5194/egusphere-2026-3599
Preprint. Discussion started: 26 June 2026

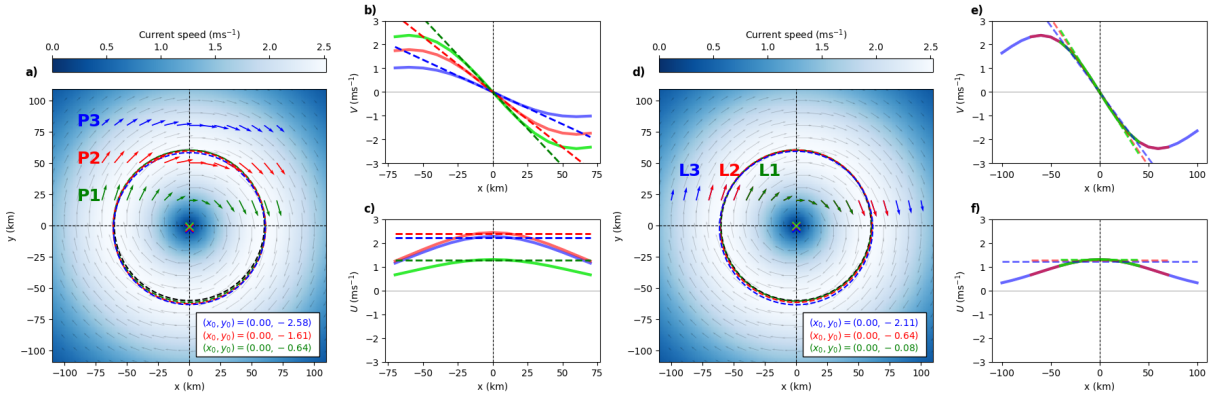

Figure 3. The SOLO method applied to an idealised axisymmetric eddy using velocities along transects with (a) varying proximities (P1–P3) to the eddy center and (d) varying transect lengths (L1–L3). Panels (b) and (c) show the across-track and along-track velocities for P1–P3, respectively, with linearisation (dotted) about the point of closest approach $x_0 = 0$. Panels (e) and (f) show the same for L1–L3. Coloured dotted ellipses in panels (a) and (b) represent the contours of maximum tangential velocity estimated for each test. The true contour of maximum tangential velocity is shown as a black dotted ellipse; however, because the estimates align closely with the true contour, it is largely indistinguishable.

peak tangential velocity. These results demonstrate that the SOLO method yields consistently accurate parameter estimates for axisymmetric eddies, despite variations in transect proximity to the inner core and transect length. This confirms SOLO as a robust tool for analysing axisymmetric eddies.

By design, the SOLO method assumes strictly axisymmetric eddies. Since ocean eddies are rarely perfectly circular, we assess the sensitivity of the method to eddy deformation by quantifying the error in the estimated eddy center as a function of aspect ratio. This analysis is shown in Figure 5, where SOLO is applied to a fixed horizontal transect across idealised eddies with aspect ratios ranging from 1 (axisymmetric) to 3. The error in the eddy center estimate increases with increasing deformation. For weakly deformed eddies (aspect ratios ≤ 1.25), the error remains below 5 km, which is small relative to typical mesoscale eddy diameters (100–200 km). For strongly deformed eddies (aspect ratio ≈ 3), the error increases to approximately 20 km.

3.1.2 Application to S-ADCP Data

We now apply the SOLO method to a straight-line transect of S-ADCP data. The method first estimates the point of closest approach, x_0, which is then refined using observations within a 30 km radius ($|x - x_0| \leq 30$ km). Velocity data satisfying $|x - x_0| \leq 30$ km of the refined x_0 are used to estimate the inner-core ESP parameters, while observations satisfying $|x - x_0| \leq 100$ km are used to determine the outer-core parameters.

https://doi.org/10.5194/egusphere-2026-3599
Preprint. Discussion started: 26 June 2026

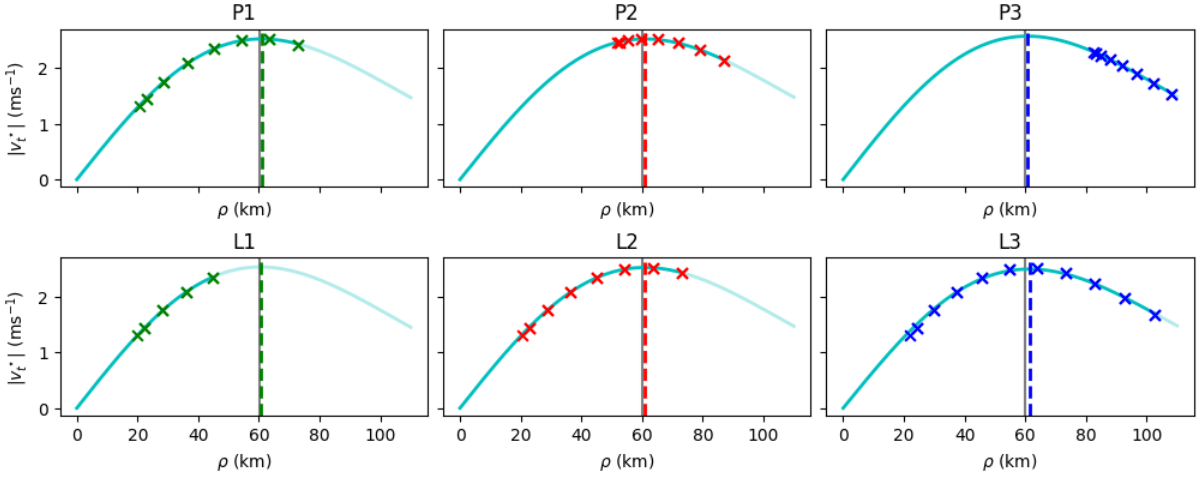

Figure 4. Normalised tangential velocity fits to the SOLO test transect data. Cross markers denote the transect velocity measurements used by the SOLO method. The solid cyan curve shows the fitted normalised tangential velocity profile Eq. (11). The curve fades beyond the outermost data point, indicating where the profile is extrapolated beyond the observations. The vertical dashed line marks the predicted location of the maximum normalised tangential velocity, while the thin black vertical line at $\rho = 60$ km indicates the true location of the maximum.

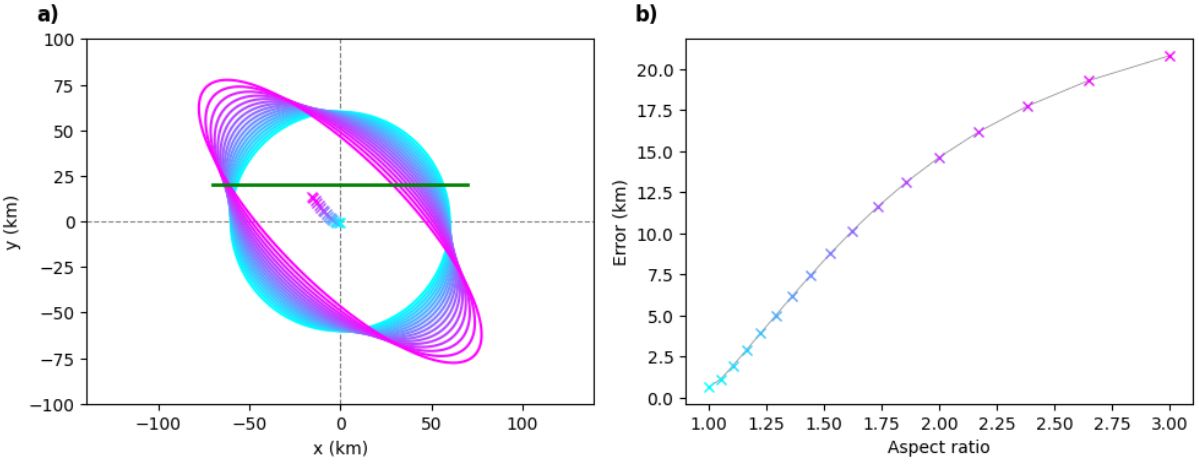

Figure 5. (a) Ellipses denote the contour of maximum tangential velocity for a sequence of two-dimensional idealised Gaussian eddies, progressing from an axisymmetric eddy (cyan) to an increasingly deformed eddy (pink). The SOLO method is applied to each eddy using the same horizontal transect (green line). Cross markers (×) indicate the SOLO-estimated eddy centers, colour-coded by eddy deformation. (b) Error in the SOLO estimate of the eddy center as a function of eddy aspect ratio.

https://doi.org/10.5194/egusphere-2026-3599
Preprint. Discussion started: 26 June 2026

Table 1. Estimated ESP parameters obtained using the SOLO method for the six tests shown in Figure 3, compared with the true (control) parameters of the idealised eddy. Reported quantities include the eddy center (x_0, y_0), angular velocity Ω, and core radius R_c.

	x_0 (km)	y_0 (km)	Ω (s^{-1})	R_c (km)
Control	0.000000e+00	0.000000	-0.000069	85.000000
P1	0.000000e+00	-0.643841	-0.000068	86.113585
P2	-7.105427e-14	-1.609602	-0.000068	86.324602
P3	0.000000e+00	-2.575363	-0.000070	85.883518
L1	2.131628e-14	-0.084143	-0.000069	85.486119
L2	0.000000e+00	-0.643841	-0.000068	86.113585
L3	-5.684342e-14	-2.113639	-0.000067	86.755294
Absolute error relative to control				
P1 Err	0.000000e+00	0.643841	9.859358e-07	1.113585
P2 Err	7.105427e-14	1.609602	1.192573e-06	1.324602
P3 Err	0.000000e+00	2.575363	5.352636e-07	0.883518
L1 Err	2.131628e-14	0.084143	2.274523e-07	0.486119
L2 Err	0.000000e+00	0.643841	9.859358e-07	1.113585
L3 Err	5.684342e-14	2.113639	2.250588e-06	1.755294

Applying the SOLO method to a quasi-straight transect of S-ADCP data yielded the following parameters: $(x_0, y_0) = (-8.7, 2.2)$ km, $\omega = -4.0 \times 10^{-5}$ s^{-1}, $\Omega = -2.0 \times 10^{-5}$ s^{-1}, $R_c = 67.2$ km, and $R^2 = 0.95$. Where R^2 is the coefficient of determination in the error between the transect data and the ESP modelled data. The resulting velocity field reconstructed from these parameters is shown in Figure 6.

3.2 DOPPIO (Double orthogonal transect)

Velocity data along a single transect is insufficient to determine the shape of an eddy because the linear least-squares fitting problem is underdetermined in this case. This limitation is removed for two-dimensional gridded data sets, for example, numerical model output, satellite data, or orthogonal shipboard transects. The DOPPIO method exploits the geometric structure of gridded data sets — in which velocity data is sampled or evaluated along two orthogonal transects – to efficiently derive the full elliptical streamfunction parameters for the eddy.

We again adopt a coordinate system aligned with the velocity sampling pattern. In this case, velocity measurements $(\hat{u}_i, \hat{v}_i)$ are taken along two orthogonal straight-line transects aligned with the x- and y-axes. The transects intersect at the origin $(0, 0)$

https://doi.org/10.5194/egusphere-2026-3599
Preprint. Discussion started: 26 June 2026

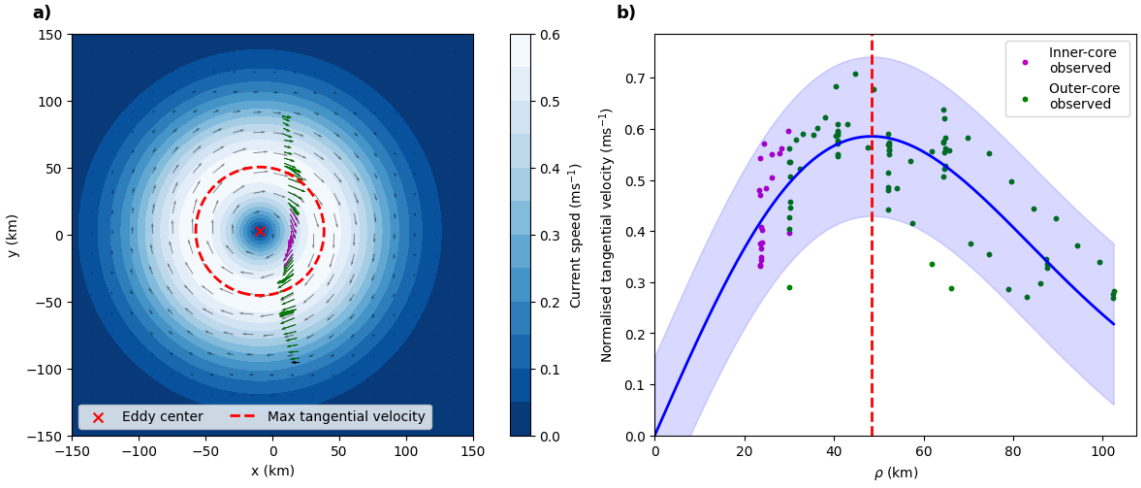

Figure 6. (a) Application of the SOLO method to a quasi-straight transect of S-ADCP data. Velocity data used to estimate the inner-core ESP parameters are shown in magenta, while velocity data used to estimate the outer-core parameters are shown in green (inclusive of the inner-core data). The background flow represents the eddy reconstructed from the S-ADCP observations using the SOLO method. (b) Normalised tangential velocity fit (11) (blue line) to observed data to derive outer-core ESP parameters. Shaded region shows 95% prediction interval.

and the eddy center is taken to be at (x_0, y_0). The modelled inner-core velocities are given by

$$u^{\text{core}}(x,0) = -\Omega\,(q_{12}(x-x_0) - q_{22}y_0)\,, \qquad v^{\text{core}}(x,0) = \Omega\,(q_{11}(x-x_0) - q_{12}y_0) \tag{17}$$

$$u^{\text{core}}(0,y) = -\Omega\,(q_{22}(y-y_0) - q_{12}x_0)\,, \qquad v^{\text{core}}(0,y) = \Omega\,(q_{12}(y-y_0) - q_{11}x_0)\,. \tag{18}$$

Following the SOLO method, we fit the along-track and across-track velocities to cubic polynomials,

$$u(x,0) = U_1(x) = \sum_{n=0}^{3} A_n (x-x_1)^n, \qquad v(x,0) = V_1(x) = \sum_{n=0}^{3} B_n (x-x_1)^n, \tag{19}$$

$$u(0,y) = U_2(y) = \sum_{n=0}^{3} C_n (y-y_1)^n, \qquad v(0,y) = V_2(y) = \sum_{n=0}^{3} D_n (y-y_1)^n, \tag{20}$$

where $(x_1, 0)$ and $(0, y_1)$ are the inflection points where the across-track velocities vanish, $V_1(x_1) = 0$ and $U_2(y_1) = 0$. Because of the ellipticity of the streamlines, the inflection points $x = x_1$ and $y = y_1$ do not match the points of closest approach along each transect, $x = x_0$ and $y = y_0$. Instead, the points of closest approach — and hence the eddy center — are inferred from the behaviour of the fitted velocity data near the inflection points.

As in the SOLO method, a cubic fit allows for a better representation of the behaviour of the velocities and their derivatives near the inflection points. However, the parameters A_n, B_n, C_n, D_n are not independent. From the definitions $V_1(x_1) = 0$ and $U_2(y_1) = 0$, we see that $B_0 = 0 = C_0$. Likewise, from (17, 18), it can be shown that $A_1 = -D_1$. Using (9), we perform a single least-squares fit of the remaining independent parameters of the cubic polynomials using all four velocity components.

https://doi.org/10.5194/egusphere-2026-3599
Preprint. Discussion started: 26 June 2026

The inner-core elliptical streamfunction parameters are then derived from the fitted data by forming the matrix of derivatives of the cubic polynomials evaluated at $x = x_1$ and $y = y_1$,

$$W = \begin{bmatrix} U_1'(x_1) & U_2'(y_1) \\ V_1'(x_1) & V_2'(y_1) \end{bmatrix} = \begin{bmatrix} A_1 & B_1 \\ C_1 & D_1 \end{bmatrix}, \tag{21}$$

with $A_1 = -D_1$ by construction, as noted above. Using the modelled core velocities (17, 18), we obtain the matrix equation

$$W = \begin{bmatrix} \Omega q_{12} & \Omega q_{22} \\ -\Omega q_{11} & -\Omega q_{12} \end{bmatrix} = \Omega J Q. \tag{22}$$

Thus, the eddy shape Q and angular velocity Ω are given by

$$\Omega = \mathrm{sgn}(B_1)\sqrt{\det W}, \qquad Q = -\Omega^{-1} J W, \tag{23}$$

where we have used $q_{22} > 0$ and $\det Q = 1$. Finally, the eddy center is obtained from

$$\boldsymbol{u}^{\mathrm{core}}(\boldsymbol{x}) = \Omega J Q(\boldsymbol{x} - \boldsymbol{x}_0) = W(\boldsymbol{x}_1 - \boldsymbol{x}_0) + W(\boldsymbol{x} - \boldsymbol{x}_1). \tag{24}$$

Evaluating this at the inflection points $(x_1, 0)$ and $(0, y_1)$ and using $U_2(y_1) = 0$ and $V_1(x_1) = 0$ then gives

$$\begin{bmatrix} U_2(y_2) \\ V_1(x_1) \end{bmatrix} = W(\boldsymbol{x}_1 - \boldsymbol{x}_0) - \begin{bmatrix} W_{11} x_1 \\ W_{22} y_1 \end{bmatrix} = 0, \tag{25}$$

from which we obtain

$$\boldsymbol{x}_0 = W^{-1} \begin{bmatrix} W_{12} y_1 \\ W_{21} x_1 \end{bmatrix}. \tag{26}$$

3.2.1 Idealized Model Validations

Examples illustrating the DOPPIO method are shown in Figure 7. Tests with transect radii of 30 km were centered at $(x, y) = (10, 10)$ km (EP1), $(x, y) = (-25, 25)$ km (EP2), and $(x, y) = (-30, -30)$ km (EP3). The closer the transects are centered to the true eddy center, the more accurately the DOPPIO method performs (Table 2, Figure 7).

Additional tests, not shown in Figure 7a, used transect radii of 20 km (EL1), 30 km (EL2), and 40 km (EL3), all centered at $(x, y) = (15, 15)$ km. The corresponding results are summarised in Table 2. Across all tests, the DOPPIO method is robust. Horizontal position errors remain below 1.1 km ($\leq 1.3\%$ of the eddy core radius), while errors in R_c remain below 3.2 km. The deformation parameter α (aspect ratio) is recovered with errors below 1×10^{-2} (except EP3), indicating accurate reconstruction of the eddy geometry.

Outer-core fits to the normalised tangential velocity for each test are shown in Figure 8. These fits show negligible errors in identifying the location of the maximum tangential velocity, except for test EP3, where the error is approximately 4 km. Errors for EP3 are expected, as the test corresponds to the transect located furthest from the eddy inner core and is required to extrapolate the across track velocity inversion points x_1 and y_1 (Figure 7d).

https://doi.org/10.5194/egusphere-2026-3599
Preprint. Discussion started: 26 June 2026

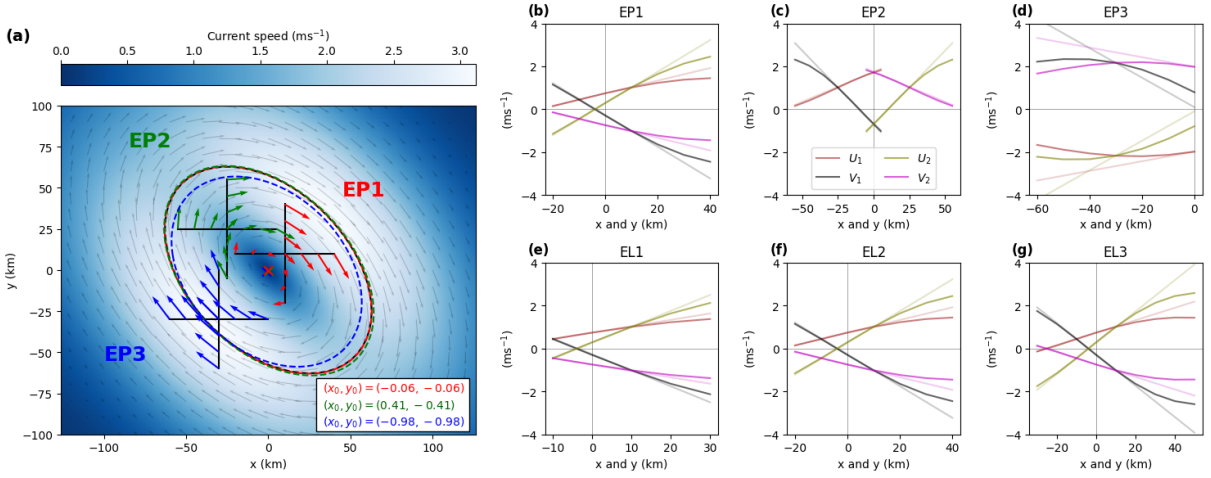

Figure 7. (a) Application of the DOPPIO method to an idealised non-axisymmetric eddy using six sets of velocity observations. Tests EP1–EP3 are shown in panel (a), while EL1–EL3 are not shown in panel (a) but their corresponding results are presented in panels (e–g). Coloured dotted ellipses in panel (a) represent the estimated contours of maximum tangential velocity for EP1–EP3. The true contour is shown as a black dotted ellipse; however, it is largely indistinguishable where the estimates closely align (particularly for EP1 and EP2). Panels (b–g) show the fitted transect velocities for all tests, along with their linearisation (faint lines) at the inflection points x_1 and y_1.

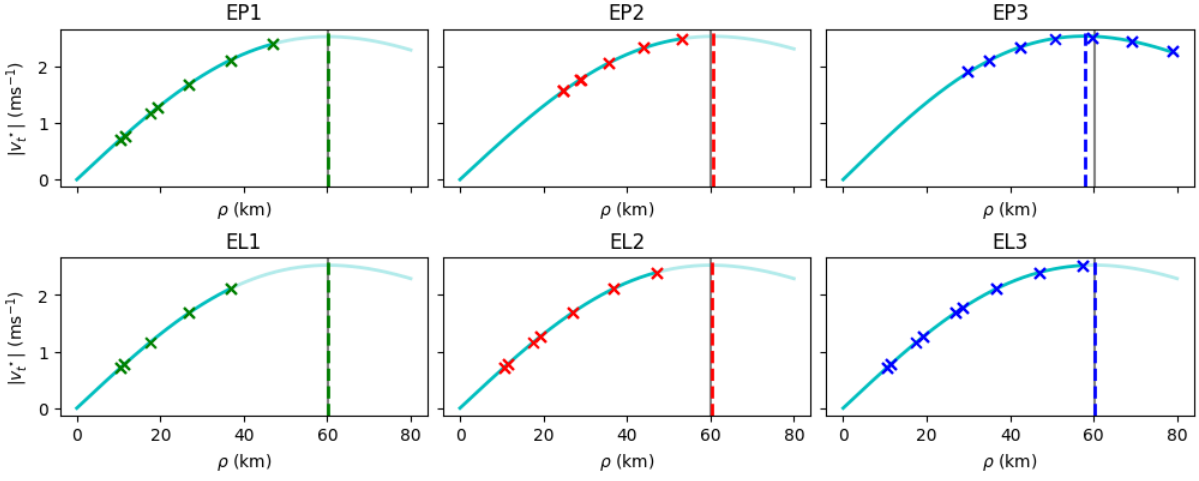

Figure 8. Same as Figure 4, but for the DOPPIO method applied to tests EP1, EP2, EP3, EL1, EL2 and EL3.

3.2.2 Application to Gridded Velocity Data

We now apply the DOPPIO method to two-dimensional, gridded surface velocity data from a numerical model within and around the CE.

https://doi.org/10.5194/egusphere-2026-3599
Preprint. Discussion started: 26 June 2026

Table 2. Estimated ESP parameters obtained using the DOPPIO method for the six tests shown in Figure 7, compared with the true (control) parameters of the idealised eddy. Reported quantities include the eddy center (x_0, y_0), inner-core vorticity ω, angular velocity Ω, aspect ratio α, and core radius R_c.

	x_0 (km)	y_0 (km)	ω (s^{-1})	Ω (s^{-1})	α	R_c (km)
Control	0.000000	0.000000	-0.000151	-0.000069	1.527525	85.000000
EP1	-0.061756	-0.061756	-0.000148	-0.000069	1.523463	85.295308
EP2	0.409749	-0.409749	-0.000138	-0.000069	1.538592	86.154608
EP3	-0.975451	-0.975451	-0.000138	-0.000077	1.402122	79.542198
EL1	-0.008558	-0.008558	-0.000149	-0.000069	1.525301	85.279697
EL2	-0.061756	-0.061756	-0.000148	-0.000069	1.523463	85.295308
EL3	-0.127344	-0.127344	-0.000146	-0.000069	1.521085	85.177156
Absolute error relative to control						
EP1 Err	0.061756	0.061756	0.000003	8.734519e-08	0.004063	0.295308
EP2 Err	0.409749	0.409749	0.000013	6.668969e-07	0.011067	1.154608
EP3 Err	0.975451	0.975451	0.000013	8.223520e-06	0.125403	5.457802
EL1 Err	0.008558	0.008558	0.000002	1.687995e-08	0.002224	0.279697
EL2 Err	0.061756	0.061756	0.000003	8.734519e-08	0.004063	0.295308
EL3 Err	0.127344	0.127344	0.000005	1.796250e-08	0.006440	0.177156

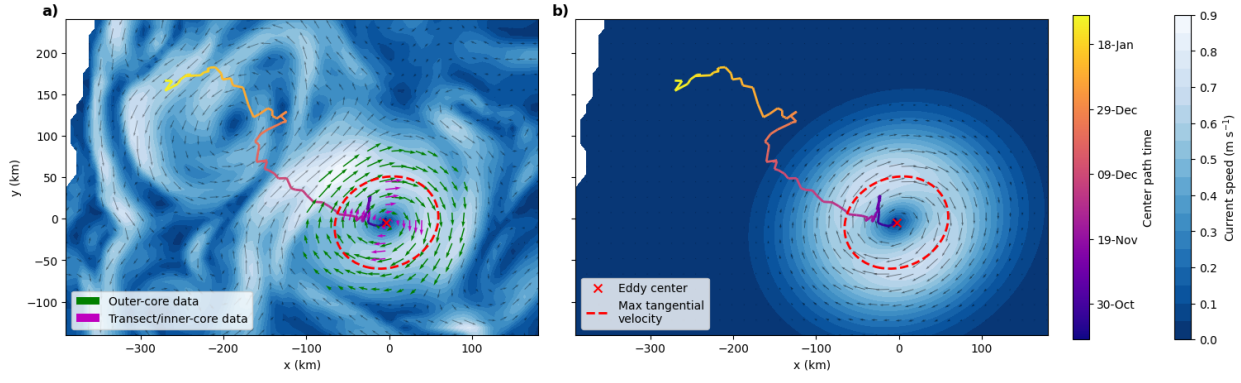

Figure 9. (a) Application of the DOPPIO method to gridded surface velocity data at timestep 2023-11-03T00. Velocity vectors are subsampled (spacing = 2) for clarity. Magenta vectors denote velocity data used for inner-core estimation, and green vectors denote data used for outer-core estimation. (b) Reconstructed eddy from the numerical data using the DOPPIO method.

The tracking and mapping procedure for the CE using the DOPPIO method is as follows:

https://doi.org/10.5194/egusphere-2026-3599
Preprint. Discussion started: 26 June 2026

1. On day 1, radial transects of length 30 km are extended outwards from the origin (the initial eddy center estimate). These transects are used to estimate the inner-core ESP parameters.

2. Using the estimated inner-core parameters, the radial coordinate ρ is calculated and all velocity data satisfying $\rho \leq 100$ km are used to determine the outer-core parameters.

3. The algorithm then advances to the next day. Radial transects are centered on the eddy center identified on the previous day, and the above steps are repeated until one of the following conditions is met: (i) the eddy center displaces by more than 100 km from the previous day, (ii) the sign of the vorticity changes relative to the first day, or (iii) the temporal record ends.

The parameters obtained from this procedure, applied to the numerical dataset, are shown in Figure 10 f, g as time series over the full tracking period. Here, R^2 denotes the coefficient of determination, computed by comparing the observed velocity data with the ESP-reconstructed velocity field at each time step. For selected timesteps, the DOPPIO-derived eddy center and contour of maximum tangential velocity are overlaid on the original numerical velocity field to assess performance.

These timesteps were chosen to capture periods of significant variation in the ESP parameters. In particular, during periods of strong deformation (e.g., Figure 10b, c, and e, where $\alpha \gtrsim 1.5$), the DOPPIO method accurately represents the elliptical structure of the flow. Overlaying the DOPPIO results on the original numerical velocity field shows that the estimated eddy centers align closely with the centers of the velocity field, while the contours of maximum tangential velocity are recovered with high accuracy. Small offsets in these contours are occasionally observed (south-west corner of Figure 10d) and are expected due to external flow influences and non ideal elliptical structure. Overall, the method provides a robust reconstruction of eddy size and deformation across a broad range of scales ($R_c > 100$ km and $R_c < 65$ km, Figure 10d, e).

3.3 LATTE (unstructured or multi-platform data)

The LATTE method is designed for unstructured or multi-platform observations. The underlying methodology is straightforward: an optimisation is performed on the (x, y, u, v) velocity data within $\mathcal{R}^{\text{core}}$ (Eq. 9) to estimate the optimal inner-core parameters x_0, y_0, Ω, and Q. In this study, the optimisation is carried out using a least-squares regression implemented with the `scipy` package (v1.15.3), although any suitable optimisation routine could be applied.

3.3.1 Idealized Model Validations

The LATTE method is demonstrated in Figure 11 using four distinct synthetic data configurations: (Ex1) a shipboard ADCP transect, (Ex2) an exaggerated drifter trajectory with corresponding velocity data, (Ex3) intersecting transects, and (Ex4) gridded velocity data. The corresponding parameter-recovery results are summarised in Table 3. Overall, LATTE exhibits moderate

https://doi.org/10.5194/egusphere-2026-3599
Preprint. Discussion started: 26 June 2026

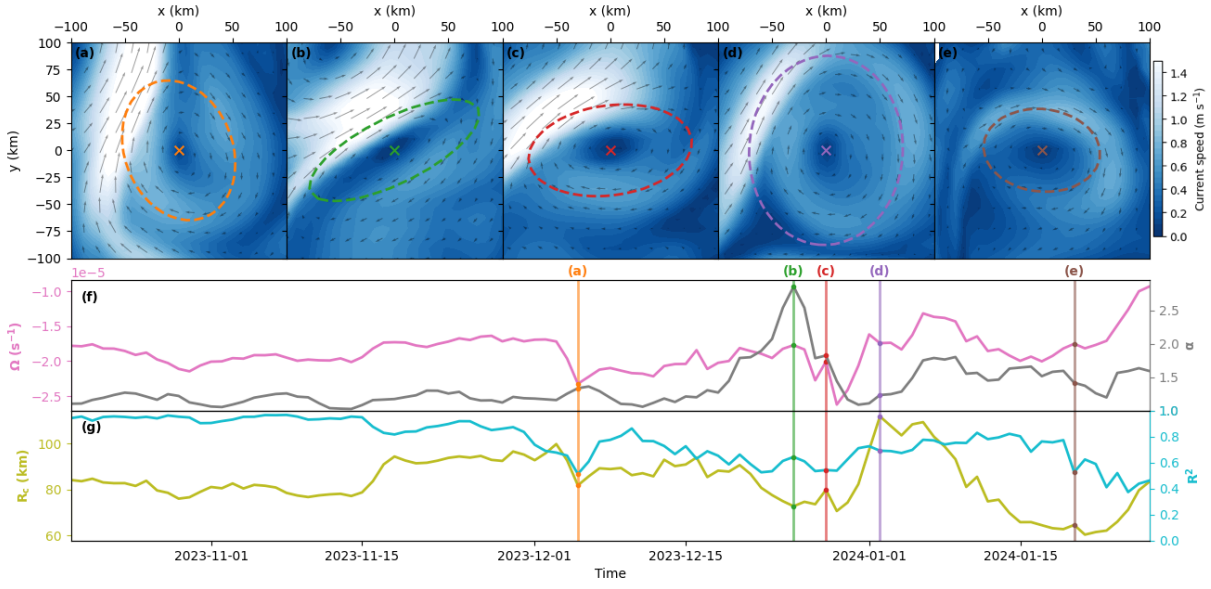

Figure 10. (a–e) The DOPPIO method results (eddy center, ×, and contour of maximum tangential velocity, dashed ellipse) overlaid on the original numerical velocity field of the CE at timesteps 2023-12-05, 2023-12-25, 2023-12-28, 2024-01-02, and 2024-01-20, respectively. (f, g) Time series of angular velocity Ω, aspect ratio α, core radius R_c, and coefficient of determination R^2 (computed by comparing the input velocity data with the reconstructed model velocity field) for the CE. The timesteps shown in (a–e) are indicated in (f, g) by vertical lines with corresponding colours.

sensitivity to perturbations; however, across all test cases (Ex1–Ex4), eddy center estimation errors remain below $1.5\ \mathrm{km}$ ($\leq 2\%$ of the eddy core radius), indicating reliable recovery of the eddy center.

As shown in Figure 11, when velocity observations lie primarily within the contour of maximum tangential velocity (e.g., Ex1–Ex4), the LATTE method successfully recovers the inner-core ESP parameters (small errors in x_0, y_0, ω, and α; Table 3) despite variations in sampling geometry and data sparsity. This result indicates that observations confined within this contour sufficiently satisfy the assumption that measurements originate from the eddy inner core, allowing accurate estimation of the inner-core structure.

Figures 11e–h further demonstrate that including velocity observations outside the eddy inner core—specifically beyond the contour of maximum tangential velocity (vertical black line)—improves estimation of the outer-core parameters (g,h). For example, Ex4 includes observations beyond the peak tangential velocity contour (Figure 11h) and yields an R_c error of only $0.1\ \mathrm{km}$, whereas Ex1, which samples primarily within the inner core (Figure 11e), produces a larger R_c error of $6.3\ \mathrm{km}$. This behaviour highlights the importance of sampling within the eddy inner core for accurate estimation of inner-core parameters, and beyond the inner core for reliable estimation of outer-core parameters.

https://doi.org/10.5194/egusphere-2026-3599
Preprint. Discussion started: 26 June 2026

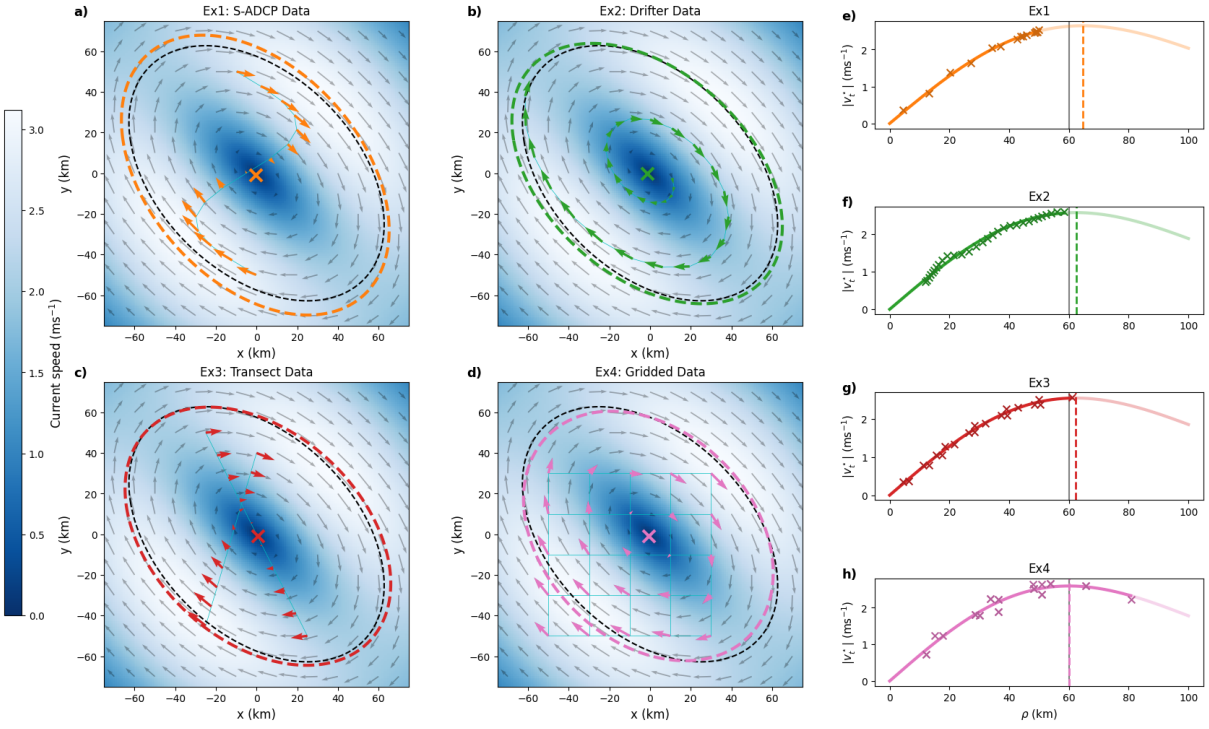

Figure 11. (a–d) Demonstration of the LATTE method applied to four distinct data configurations. The black dotted ellipse represents the true contour of maximum tangential velocity, while the coloured ellipses show the LATTE method's approximated contour of maximum tangential velocity. (e–h) Normalised tangential velocities predicted by the LATTE method using the velocity data shown in (a–d). Scattered $\times$ markers represent velocity observations input into the LATTE method. The vertical black line indicates where the true maximum normalised tangential velocity occurs.

3.3.2 Application to multi-platform data (S-ADCP and satellite)

Here we demonstrate the application of the LATTE method applied to a multi-platform dataset consisting of S-ADCP (near-surface) observations (taken over a 4.5 day period) and satellite-derived surface velocity data.

The parameter estimation procedure using the LATTE method is as follows:

1. Velocity observations within a radius of 30 km from the initial center estimate $(0, 0)$ are used as input to LATTE to compute an initial set of inner-core ESP parameters. These parameters are then used to reselect an optimised subset of data points satisfying $\rho \leq 30$ km, which are used to recompute the inner-core parameters.

2. All velocity observations satisfying $\rho \leq 100$ km are then used to determine the outer-core parameters (Figure 12c).

https://doi.org/10.5194/egusphere-2026-3599
Preprint. Discussion started: 26 June 2026

Table 3. Estimated ESP parameters obtained using the LATTE method for the four tests shown in Figure 11, compared with the true (control) parameters of the idealised eddy. Reported quantities include the eddy center (x_0, y_0), inner-core vorticity ω, angular velocity Ω, aspect ratio α, and core radius R_c.

	x_0 (km)	y_0 (km)	ω (s^{-1})	Ω (s^{-1})	α	R_c (km)
Control	0.000000	0.000000	-0.000151	-0.000069	1.527525	85.000000
Ex1	-0.610966	-0.924386	-0.000147	-0.000068	1.518957	91.331040
Ex2	-1.445990	-0.161871	-0.000149	-0.000068	1.541855	88.256970
Ex3	0.666927	-0.949101	-0.000145	-0.000067	1.470733	87.909594
Ex4	-0.840778	-0.840778	-0.000149	-0.000071	1.355681	84.896625
Absolute error relative to control						
Ex1 Err	0.610966	0.924386	0.000004	0.000002	0.008568	6.331040
Ex2 Err	1.445990	0.161871	0.000002	0.000001	0.014329	3.256970
Ex3 Err	0.666927	0.949101	0.000006	0.000002	0.056792	2.909594
Ex4 Err	0.840778	0.840778	0.000002	0.000002	0.171844	0.103375

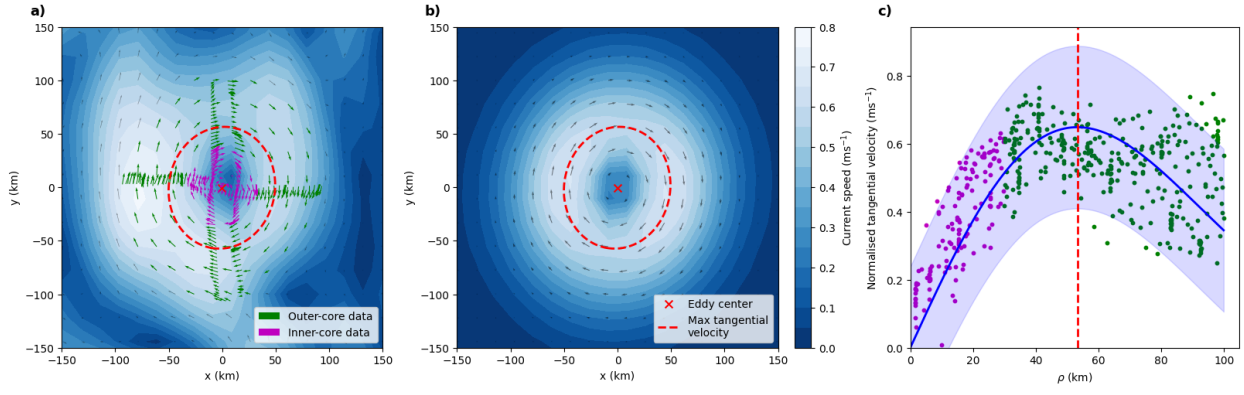

Figure 12. (a) Application of the LATTE method to multi-platform velocity data consisting of near surface S-ADCP observations together with background satellite velocity data interpolated at the mean S-ADCP observation time (2023-10-19T16:30). Velocity data used to estimate the inner-core ESP parameters are shown in magenta, while velocity data used to estimate the outer-core parameters are shown in green (inclusive of the inner-core data). (b) The reconstructed eddy obtained from the multi-platform dataset using the LATTE method. (c) Normalised tangential velocity fit (11) (blue line) to observed data to derive outer-core ESP parameters. Shaded area shows 95% prediction interval.

Applying the LATTE method to the multi-platform dataset (combining S-ADCP and satellite observations) yielded the following parameters: $(x_0, y_0) = (-0.4, -0.4)$ km (relative to (154.3°E, 37.9°S)), $\omega = -4.1\times, 10^{-5}$ s^{-1}, $\Omega = -1.9 \times 10^{-5}$ s^{-1},

https://doi.org/10.5194/egusphere-2026-3599
Preprint. Discussion started: 26 June 2026

$\alpha = 1.15$, $R_c = 75.3$ km, and $R^2 = 0.91$. Where R^2 is the coefficient of determination in the error between the transect data and the ESP modelled data. The velocity field reconstructed from these parameters is shown in Figure 12b.

3.3.3 Application to multi-platform data (drifter and satellite)

We now apply the LATTE method to another multi-platform dataset consisting of Lagrangian drifter velocity observations and satellite-derived surface velocity data.

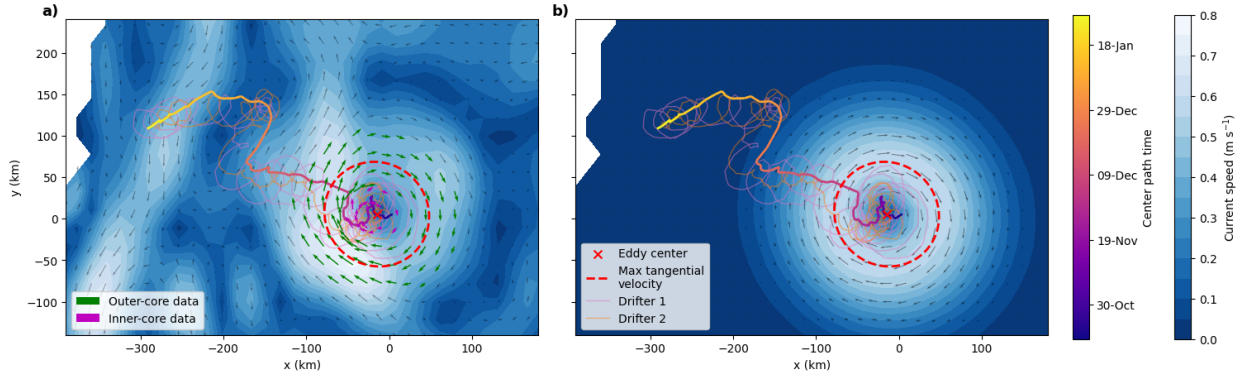

Figure 13. (a) Application of the LATTE method to multi-platform velocity data at timestep 2023-10-29T06, consisting of satellite velocity data and local drifter velocity observations within a ± 1 day window. Velocity data used to estimate the inner-core ESP parameters are shown in magenta, while velocity data used to estimate the outer-core parameters are shown in green (inclusive of the inner-core data). (b) The reconstructed eddy obtained from the multi-platform data using the LATTE method. Drifter trajectories over the full observation period are shown, together with the eddy center trajectory over the same period as inferred from the multi-platform analysis.

The tracking and mapping procedure for the CE using the LATTE method with the drifter–satellite multi-platform dataset is as follows:

1. On day 1, velocity observations within a radius of 30 km from the initial center estimate $(0,0)$ are used as input to LATTE to compute an initial set of inner-core ESP parameters.
2. An optimised subset of observations satisfying $\rho \leq 30$ km is then selected, and the inner-core parameters for that day are recomputed.
3. Velocity observations satisfying $\rho \leq 100$ km are then used to estimate the outer-core parameters.
4. The algorithm advances to the next day. Velocity observations within $\rho \leq 30$ km of the previous day's center are selected, and steps 2–4 are repeated. The tracking continues until one of the following conditions is met: (i) the eddy center displaces by more than 100 km relative to the previous day, (ii) the sign of the vorticity changes relative to the first day, or (iii) the temporal record ends.

https://doi.org/10.5194/egusphere-2026-3599
Preprint. Discussion started: 26 June 2026

The parameters obtained from this procedure applied to the multi-platform dataset are shown in Figure 14 as time series over the full tracking period. Here, R^2 denotes the coefficient of determination between the observed velocity data and the ESP-reconstructed velocity field at each time step. For comparison, parameters derived using drifter-only data are also shown.

When using drifter data alone, the analysis is effectively restricted to inner-core ESP parameters, as drifters rarely sample beyond the contour of maximum tangential velocity. Consequently, outer-core parameters (e.g., R_c) cannot be reliably estimated, preventing full reconstruction of the velocity field and hence calculation of R^2.

The results demonstrate that combining drifter and satellite data reduces noise in the parameter estimates, notably eliminating large spikes present in the drifter-only results (e.g., around 2023-11-15). The multi-platform estimates closely follow those obtained from numerical data using the DOPPIO method, indicating that the inclusion of satellite data stabilises the ESP parameter recovery. Importantly, the multi-platform approach enables estimation of outer-core parameters and full velocity-field reconstruction, which is not possible using drifter data alone.

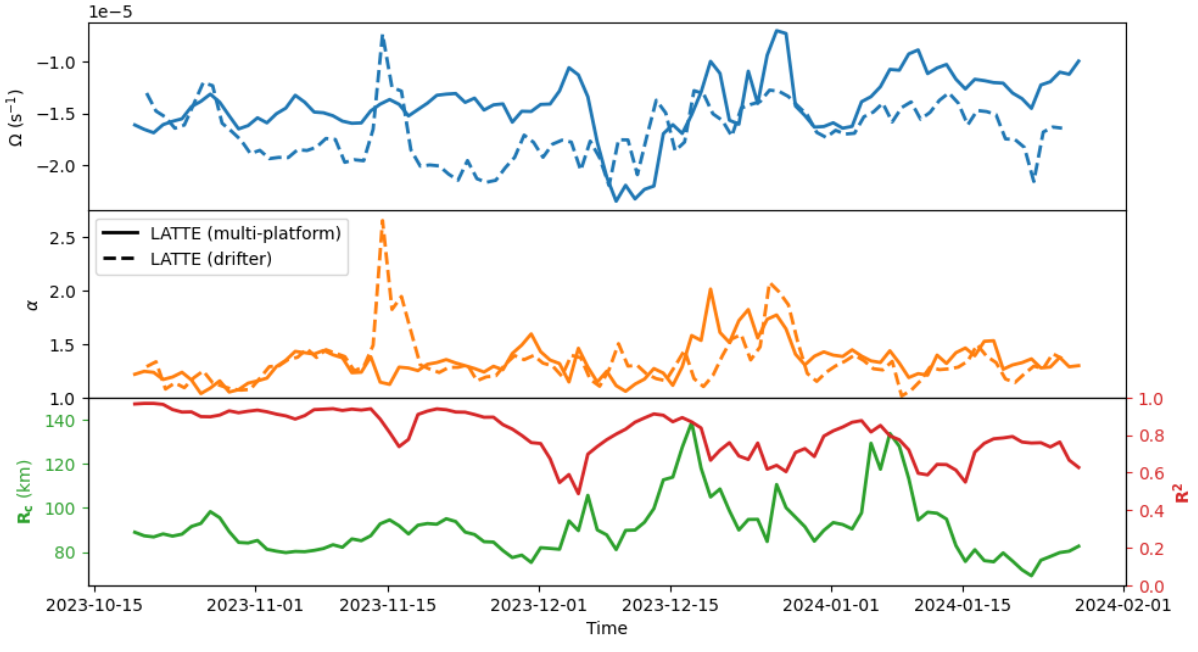

Figure 14. Time series of angular velocity Ω, aspect ratio α, core radius R_c, and coefficient of determination R^2 (computed by comparing input velocity data with the reconstructed model velocity field) for the CE. Solid lines show LATTE estimates from multi-platform observations (drifter and satellite velocity data, Figure 13), while dashed solid lines show LATTE estimates using drifter-only velocity data.

https://doi.org/10.5194/egusphere-2026-3599
Preprint. Discussion started: 26 June 2026

4 Discussion and Conclusion

The need for robust and flexible methods to characterise ocean eddies across diverse observational sampling patterns has been widely recognised in the literature. Existing approaches have largely been developed for specific data types—such as gridded fields (Nencioli et al., 2010; Chelton et al., 2011), transects (Roughan et al., 2017), or Lagrangian trajectories (Lilly et al., 2011; Lilly and Pérez-Brunius, 2021)—which limits their ability to integrate multi-platform observations or to provide a consistent description of eddy structure. In this study, we address this limitation by introducing a unified geometric framework, the *Elliptical Streamfunction Parametrisation* (ESP), which enables the reconstruction of eddy properties from arbitrary sampling patterns.

A key advantage of the ESPresso framework is that it generalises existing geometric approaches by explicitly allowing for non-axisymmetric structure. Many prior methods, including MOCA (Roughan et al., 2017) and related axisymmetric models (Luce and Rossby, 2008; Belkin et al., 2020), rely on assumptions of circular symmetry that are only valid within the inner core of an eddy. As demonstrated in this study (Figure 5), such assumptions introduce systematic errors when applied to non-axisymmetric vortices. By contrast, the ESP framework directly incorporates deformation through its elliptical representation, enabling more accurate recovery of eddy geometry and dynamics across both inner- and outer-core regions.

Within this framework, the SOLO, DOPPIO, and LATTE methods provide complementary approaches tailored to different observational configurations. The SOLO method remains effective for single transects when the flow is approximately axisymmetric (Figure 5) and the sampling passes near the eddy center (Figure 3), consistent with earlier approaches (Roughan et al., 2017), but with improved robustness through selective use of inner-core observations (Figure 2). In this study, application of the SOLO method to S-ADCP observations (with a temporal extent of approximately one day) across a cyclonic eddy (CE) achieved a strong reconstruction ($R^2 = 0.95$) (Figure 6). When applied independently across depth levels (possible using S-ADCP data), the method enables reconstruction of the horizontal velocity structure throughout the water column. This provides a pathway for resolving three-dimensional eddy structure and associated dynamical properties, and represents a promising direction for future work.

The DOPPIO method extends this capability to non-axisymmetric eddies by exploiting two intersecting transects, making it particularly well suited to regularly gridded datasets such as numerical model output or satellite-derived velocity fields. By ensuring that observations sample the eddy inner core and explicitly accounting for eddy deformation, the DOPPIO method improves parameter estimation accuracy (Figure 7, Table 4) and provides a robust framework for tracking eddy evolution in both time and depth.

In the present study, the DOPPIO method achieved consistently high agreement with the observed velocity field ($R^2 \gtrsim 0.75$) across time, enabling mapping of the evolving spatio-temporal structure of the CE (Figures 9, 10). This was achieved by se-

https://doi.org/10.5194/egusphere-2026-3599
Preprint. Discussion started: 26 June 2026

quentially applying the method to gridded surface velocity data from a numerical model: orthogonal transects of length 30 km were centered on an initial eddy location to estimate inner-core ESP parameters, which were then used to identify outer-core observations ($\rho \leq 100$ km). The procedure (Figure 1) was advanced in time by recentering the transects on the previously estimated eddy center and repeating the analysis, with tracking terminated when displacement, vorticity consistency, or temporal limits were violated. The same framework can be extended vertically by applying the method across depth levels, enabling reconstruction of the full three-dimensional velocity structure of the eddy.

Overlaying the DOPPIO results on the original numerical velocity field demonstrates that the estimated eddy centers and contours of maximum tangential velocity closely match the underlying flow structure, even during periods of strong deformation ($\alpha \gtrsim 2$, Figures 10b, c) and across a wide range of eddy sizes ($R_c > 100$ km and $R_c < 65$ km).

Although formulated using *orthogonal* transects, as naturally arises in gridded data, the method can be generalised to transects intersecting at arbitrary angles by modifying the expected transect velocity relationships (Eq. (17)) to account for transect orientation relative to the eddy.

The LATTE method provides the most flexible framework, enabling estimation of eddy properties from irregular and multi-platform datasets (Figure 11). This represents a significant advance over existing approaches for Lagrangian or sparse observations (Lilly et al., 2011; Lilly and Pérez-Brunius, 2021; Brassington, 2010), which typically infer only partial eddy properties or rely on assumptions about trajectory coherence. A key strength of LATTE is its ability to integrate heterogeneous datasets with complementary sampling characteristics, allowing robust recovery of both inner- and outer-core ESP parameters.

This capability is demonstrated through multi-platform applications to the CE. In the case of S-ADCP and satellite data (Figure 12), the complementary sampling characteristics—dense inner core coverage from S-ADCP and broader outer-core coverage from satellite observations—enable robust estimation of both inner- and outer-core ESP parameters. The resulting reconstruction achieves strong agreement with observations ($R^2 = 0.91$), demonstrating that LATTE can integrate fundamentally different data types into a consistent and physically meaningful eddy representation.

A similar behaviour is observed for the drifter–satellite application (Figure 13). Drifter observations provide dense sampling within the eddy inner core but typically lack outer-core coverage, preventing reliable estimation of parameters such as R_c and ψ_0 and hence full velocity-field reconstruction when used alone. By incorporating satellite-derived velocities, which provide broader spatial coverage, the full set of ESP parameters can be recovered. The resulting parameter estimates (Figure 14) exhibit strong agreement with the observed velocity field ($R^2 \gtrsim 0.75$) and reduced spurious variability (e.g., the spike around 2023-11-15 observed in drifter-only results).

Together, these results demonstrate that LATTE leverages the complementary strengths of multi-platform datasets to stabilise

https://doi.org/10.5194/egusphere-2026-3599
Preprint. Discussion started: 26 June 2026

parameter estimation, recover outer-core structure, and enable full reconstruction of the eddy velocity field—capabilities that are not achievable using sparse or single-platform observations alone.

Although the LATTE method is the most versatile approach, the SOLO and DOPPIO methods remain preferable when their respective sampling assumptions are satisfied. The SOLO method leverages the geometry of a single transect to robustly estimate inner-core parameters for quasi-axisymmetric eddies (Figure 5), while the DOPPIO method directly targets the eddy center using two transects and is therefore better suited when observations form orthogonal sampling patterns. To quantify the advantage of DOPPIO under such conditions, we applied the LATTE method to the EP1-EP3 and EL1-EL3 test cases and compared the resulting ESP parameters with those obtained using DOPPIO. Across most parameters and test cases, DOPPIO achieves substantial reductions in estimation error relative to LATTE, with typical improvements of order 90% (Table 4). The primary exception is the vorticity (ω), for which LATTE can yield lower errors in specific scenarios, particularly when applied close to the eddy center (EP1) or when denser observational constraints are available (EL2 and EL3). However, DOPPIO maintains consistently low absolute errors in ω ($< 5 \times 10^{-6}$ s^{-1}) relative to the true solution (Table 2), indicating stable performance even in cases where LATTE performs well.

Beyond instantaneous mapping, a major strength of the ESPresso framework is its ability to reconstruct the three-dimensional and time-evolving structure of eddies. By applying the method across depth levels or sequential time steps, it becomes possible to quantify properties such as vertical tilt, deformation, and propagation. In particular, the framework provides a practical and data-efficient means of estimating eddy tilt from partial velocity observations, which has traditionally been difficult to measure and is often inferred indirectly (Zhang et al., 2016; Roughan et al., 2017; Belkin et al., 2020; Men et al., 2024). Given the growing recognition of tilt as a dynamically significant property influencing vertical transport and biogeochemical exchange (Yang et al., 2020; Li et al., 2022a, b, 2023), this represents a key capability of the ESPresso framework.

Despite these advantages, several limitations should be acknowledged. The ESPresso framework assumes that the velocity field is well represented by elliptical streamlines, which may not hold in strongly sheared environments or during eddy–eddy interactions. In addition, the accuracy of the methods depends on the spatial distribution of observations, with insufficient outer-core sampling leading to biases in estimated eddy size and deformation (Figures 3, 7, 11). Furthermore, the current implementation does not explicitly account for ageostrophic processes, such as Ekman flows, which may influence velocity observations near the surface.

A further limitation arises from the temporal sampling of observational data. Velocity observations used in SOLO and LATTE are often collected over finite time windows rather than representing an instantaneous snapshot of the flow. For example, in this study, drifter data were aggregated over ± 1 day windows for LATTE application (Figure 13), while S-ADCP transects spanned approximately 1 and 4.5 days for SOLO and LATTE applications, respectively (Figures 6, 12). This approach assumes that the eddy does not evolve significantly over the sampling period, which is generally reasonable for mesoscale eddies; however, tem-

https://doi.org/10.5194/egusphere-2026-3599
Preprint. Discussion started: 26 June 2026

Table 4. Percentage reduction in parameter estimation error achieved by DOPPIO relative to LATTE for tests EP1-EP3 and EL1-EL3. Errors are defined relative to the control solution, with center error computed as the Euclidean distance between the estimated and control centers. For each parameter, the reported percentage is calculated as $100(\epsilon_{\mathrm{LATTE}} - \epsilon_{\mathrm{DOPPIO}})/\epsilon_{\mathrm{LATTE}}$, such that positive values indicate improved performance of DOPPIO and negative values indicate worse performance. Percentage improvements are omitted where the difference in error between the two methods is smaller than a prescribed threshold, as relative comparisons are not practically meaningful in these cases. The thresholds applied are 1 km for center and R_c, 10^{-7} s^{-1} for ω and Ω, and 5×10^{-3} for α. Mean values are computed over the remaining reported entries in each column.

	(x_0, y_0) (%)	ω (%)	Ω (%)	α (%)	R_c (%)
EP1	–	-20.9	–	93.8	93.0
EP2	94.4	7.5	93.2	94.7	94.6
EP3	98.7	86.2	80.7	51.4	98.1
EL1	–	75.4	99.4	96.6	98.4
EL2	–	-20.9	–	93.8	93.0
EL3	–	-1000.2	98.1	90.2	87.5
Mean	96.6	-145.5	92.8	86.8	94.1

poral evolution within the sampling window may introduce additional uncertainty in the estimated parameters. Minimising the temporal window is therefore desirable to ensure that the velocity data correspond as closely as possible to a single eddy state. This limitation is particularly relevant for transect-based (SOLO) and multimodal (LATTE) applications, while for DOPPIO, which operates on instantaneous gridded fields, similar considerations arise when temporally aggregated data are used.

These limitations motivate several directions for future work. In particular, addressing temporal sampling and observational sparsity will be important for extending the framework to larger and more heterogeneous datasets. While the present study demonstrates the capability of ESPresso to estimate eddy tilt, a natural next step is its systematic application across large observational and numerical datasets to develop regional and global tilt climatologies (Li et al., 2022a). Coupling such analyses with dynamical diagnostics, such as the quasi-geostrophic omega equation, would provide further insight into the mechanisms governing tilt and its role in vertical transport. More broadly, incorporating additional physical constraints, such as geostrophic balance or background shear, and integrating data-assimilation approaches may improve the physical consistency and robustness of the reconstructed velocity fields.

From a practical perspective, the results of this study suggest clear methodological recommendations. The SOLO method is well suited to single transects passing near the eddy center, the DOPPIO method is preferred for gridded velocity fields due to its improved accuracy and stability, and the LATTE method provides the greatest flexibility for irregular or multi-platform datasets.

https://doi.org/10.5194/egusphere-2026-3599
Preprint. Discussion started: 26 June 2026

Overall, the ESPresso framework provides a unified, threshold-free, and data-efficient approach for mapping and characterising ocean eddies across a wide range of observational scenarios. By enabling consistent estimation of both geometric and dynamical properties—including non-axisymmetric structure, three-dimensional evolution, and vertical tilt—this framework represents a significant advance in the quantitative analysis of mesoscale eddies.

Code and data availability. The complete Python code used in this study, including implementations of the SOLO, DOPPIO, and LATTE methods, together with the datasets required to reproduce the results, is archived on Dowse (2026) and available at https://doi.org/10.5281/zenodo.19364198. This repository provides a permanent, citable record containing all materials necessary to reproduce the results presented in this paper.

The original sources of the datasets included in the Zenodo archive are listed below:

Satellite: Australian Ocean Data Network (2026), https://thredds.aodn.org.au/thredds/catalog/IMOS/OceanCurrent/GSLA/DM/catalog.html

Drifter: Drifters 300534062034380 and 300534062784620, available from the NOAA Observing System Monitoring Center (OSMC), https://viz.pmel.noaa.gov/osmc/?color_by=platform_type

Mercator: E.U. Copernicus Marine Service Information (CMEMS) (2024), https://marine.copernicus.eu/access-data/

S-ADCP: CSIRO Marine National Facility Voyage IN2023_V06, https://www.marine.csiro.au/data/trawler/survey_details.cfm?survey=IN2023_V06

Author contributions. R.D. developed the methodology, performed the analysis, and wrote the manuscript. S.K. contributed to the conceptual development of the study and provided substantial input on methodology and manuscript editing. M.R. contributed to manuscript structure and provided editorial feedback. All authors reviewed and approved the final manuscript.

Competing interests. The authors declare that they have no competing interests.

Acknowledgements. This research includes computations using the computational cluster Katana supported by Research Technology Services at UNSW Sydney. https://doi.org/10.26190/669x-a286.

S-ADCP and drifter data used in this research were collected during a voyage aboard the *RV Investigator*, supported by a grant of sea

https://doi.org/10.5194/egusphere-2026-3599
Preprint. Discussion started: 26 June 2026

time from the CSIRO Marine National Facility (https://ror.org/01mae9353). We thank the crew, officers and support staff for their dedication and support of this work, along with the dedicated team of volunteer scientists on board.

Satellite data were sourced from Australia's Integrated Marine Observing System (IMOS), enabled by the National Collaborative Research Infrastructure Strategy (NCRIS).

This study used numerical output from the E.U. Copernicus Marine Service Information (https://doi.org/10.48670/moi-00016).

Drifter trajectories and velocities were obtained from the NOAA Observing System Monitoring Center (OSMC) and the Global Drifter Program (GDP). We thank R. Lumpkin for providing drifters for deployment during the voyage.

This research was supported by the Australian Research Council Discovery Grant #DP2301000505 and Industry Linkage Grant #LP220100515 awarded to MR and SK.

https://doi.org/10.5194/egusphere-2026-3599
Preprint. Discussion started: 26 June 2026

References

Australian Ocean Data Network: Ocean Currents, https://oceancurrent.aodn.org.au/sst.php?link=SE/latest.html, 2026.

Azaneu, M. V. C., Roughan, M., Keating, S. R., Schaeffer, A., and Schallenberg, C.: Characterising submesoscale processes, uplift and subduction across diverse fronts in the East Australian Current System, submitted to Prog. Oceanogr., 2025.

Basdevant, C. and Philipovitch, T.: On the validity of the "Weiss criterion" in two-dimensional turbulence, Physica D: Nonlinear Phenomena, 73, 17–30, 1994.

Belkin, I., Foppert, A., Rossby, T., Fontana, S., and Kincaid, C.: A Double-Thermostad Warm-Core Ring of the Gulf Stream, Journal of Physical Oceanography, 50, 489 – 507, https://doi.org/10.1175/JPO-D-18-0275.1, 2020.

Benitez-Nelson, C. R., Bidigare, R. R., Dickey, T. D., Landry, M. R., Leonard, C. L., Brown, S. L., Nencioli, F., Rii, Y. M., Maiti, K., Becker, J. W., Bibby, T. S., Black, W., Cai, W.-J., Carlson, C. A., Chen, F., Kuwahara, V. S., Mahaffey, C., McAndrew, P. M., Quay, P. D., Rappé, M. S., Selph, K. E., Simmons, M. P., and Yang, E. J.: Mesoscale Eddies Drive Increased Silica Export in the Subtropical Pacific Ocean, Science, 316, 1017–1021, https://doi.org/10.1126/science.1136221, 2007.

Brassington, G. B.: Estimating Surface Divergence of Ocean Eddies Using Observed Trajectories from a Surface Drifting Buoy, Journal of Atmospheric and Oceanic Technology, 27, 705 – 720, https://doi.org/10.1175/2009JTECHO651.1, 2010.

Cetina-Heredia, P., Roughan, M., Sebille, E., Keating, S., and Brassington, G. B.: Retention and Leakage of Water by Mesoscale Eddies in the East Australian Current System, Journal of Geophysical Research: Oceans, 124, 2485–2500, https://doi.org/10.1029/2018JC014482, 2019.

Chaigneau, A., Gizolme, A., and Grados, C.: Mesoscale eddies off Peru in altimeter records: Identification algorithms and eddy spatio-temporal patterns, Progress in Oceanography, 79, 106–119, https://doi.org/https://doi.org/10.1016/j.pocean.2008.10.013, the Northern Humboldt Current System: Ocean Dynamics, Ecosystem Processes, and Fisheries, 2008.

Chelton, D. B., Schlax, M. G., Samelson, R. M., and de Szoeke, R. A.: Global observations of large oceanic eddies, Geophysical Research Letters, 34, https://doi.org/https://doi.org/10.1029/2007GL030812, 2007.

Chelton, D. B., Schlax, M. G., and Samelson, R. M.: Global observations of nonlinear mesoscale eddies, Progress in Oceanography, 91, 167–216, https://doi.org/10.1016/j.pocean.2011.01.002, 2011.

Dowse, R.: regdowse/elliptical_streamfunction_parametrisation : ESP, https://doi.org/10.5281/zenodo.19364198, 2026.

E.U. Copernicus Marine Service Information (CMEMS): Global Ocean Physics Analysis and Forecast, https://doi.org/10.48670/moi-00016, accessed on 24 Oct 2025., 2024.

Falkowski, P. G., Ziemann, D., Kolber, Z., and Bienfang, P. K.: Role of eddy pumping in enhancing primary production in the ocean, Nature, 352, 55–58, https://doi.org/10.1038/352055a0, 1991.

Garabato, A.: A perspective on the future of physical oceanography, Philosophical Transactions of the Royal Society a Mathematical Physical and Engineering Sciences, 370, 5480–5511, https://doi.org/10.1098/rsta.2012.0400, 2012.

Gnanadesikan, A., Bianchi, D., and Pradal, M.-A.: Critical role for mesoscale eddy diffusion in supplying oxygen to hypoxic ocean waters, Geophysical Research Letters, 40, 5194–5198, https://doi.org/10.1002/grl.50998, 2013.

Griffa, A., Lumpkin, R., and Veneziani, M.: Cyclonic and anticyclonic motion in the upper ocean, Geophysical Research Letters, 35, https://doi.org/https://doi.org/10.1029/2007GL032100, 2008.

https://doi.org/10.5194/egusphere-2026-3599
Preprint. Discussion started: 26 June 2026

Hsu, P.-C., Lee, H.-J., Zheng, Q., Lai, J.-W., Su, F., and Ho, C.-R.: Tide-Induced Periodic Sea Surface Temperature Drops in the Coral Reef Area of Nanwan Bay, Southern Taiwan, Journal of Geophysical Research: Oceans, 125, e2019JC015 226, https://doi.org/10.1029/2019JC015226, 2020.

Isern-Fontanet, J., García-Ladona, E., and Font, J.: Identification of Marine Eddies from Altimetric Maps, Journal of Atmospheric and Oceanic Technology, 20, 772 – 778, https://doi.org/10.1175/1520-0426(2003)20<772:IOMEFA>2.0.CO;2, 2003.

Jin, Y., Jin, M., Wang, D., and Dong, C.: Statistical Analysis of Multi-Year South China Sea Eddies and Exploration of Eddy Classification, Remote Sensing, 16, https://doi.org/10.3390/rs16101818, 2024.

Klein, P., Lapeyre, G., Siegelman, L., Qiu, B., Fu, L., Torres, H., Su, Z., Menemenlis, D., and Gentil, S.: Ocean-Scale Interactions From Space, Earth and Space Science, 6, 795–817, https://doi.org/10.1029/2018ea000492, 2019.

Li, H., Xu, F., and Wang, G.: Global Mapping of Mesoscale Eddy Vertical Tilt, Journal of Geophysical Research: Oceans, 127, e2022JC019 131, https://doi.org/https://doi.org/10.1029/2022JC019131, e2022JC019131 2022JC019131, 2022a.

Li, H., Xu, F., Wang, G., and Shi, R.: A Multi-Layer Linear Rossby Wave Dispersion Relation for Vertical Tilt of Mesoscale Eddies, Journal of Geophysical Research: Oceans, 127, e2022JC018 703, https://doi.org/https://doi.org/10.1029/2022JC018703, e2022JC018703 2022JC018703, 2022b.

Li, H., Xu, F., Wang, G., and Shi, R.: Numerical studies of the tilting of mesoscale eddies: The effects of rotation and stratification, Deep Sea Research Part I: Oceanographic Research Papers, 191, 103 945, https://doi.org/https://doi.org/10.1016/j.dsr.2022.103945, 2023.

Li, J., Kerry, C., and Roughan, M.: A High-Resolution, Multi-Decadal, Free-Running, Hydrodynamic Simulation of the East Australia Current System Using the Regional Ocean Modeling System (Version 3.0, 1994-2019), https://doi.org/10.5281/zenodo.12703063, 2024.

Lilly, J. M. and Pérez-Brunius, P.: Extracting Statistically Significant Eddy Signals from Large Lagrangian Datasets Using Wavelet Ridge Analysis, with Application to the Gulf of Mexico, 28, 181–212, https://doi.org/10.5194/npg-28-181-2021, 2021.

Lilly, J. M., Scott, R. K., and Olhede, S. C.: Extracting waves and vortices from Lagrangian trajectories, Geophysical Research Letters, 38, https://doi.org/https://doi.org/10.1029/2011GL049727, 2011.

Luce, D. L. and Rossby, T.: On the size and distribution of rings and coherent vortices in the Sargasso Sea, Journal of Geophysical Research: Oceans, 113, https://doi.org/https://doi.org/10.1029/2007JC004171, 2008.

Mahadevan, A.: The Impact of Submesoscale Physics on Primary Productivity of Plankton, Annual Review of Marine Science, 8, 161–184, https://doi.org/10.1146/annurev-marine-010814-015912, 2016.

Matisons, L., Roughan, M., and Schaeffer, A.: Dispersion characteristics in the East Australian Current system: Insights from 20 years of Lagrangian drifter data, Progress in Oceanography, 236, 103 498, https://doi.org/https://doi.org/10.1016/j.pocean.2025.103498, 2025.

McGillicuddy, D. J., Robinson, A. R., Siegel, D. A., Jannasch, H. W., Johnson, R., Dickey, T. D., McNeil, J., Michaels, A. F., and Knap, A. H.: Influence of mesoscale eddies on new production in the Sargasso Sea, Nature, 394, 263–266, https://doi.org/10.1038/28367, 1998.

McNeil, J. D., Jannasch, H. W., Dickey, T., McGillicuddy, D., Brzezinski, M., and Sakamoto, C. M.: New chemical, bio-optical and physical observations of upper ocean response to the passage of a mesoscale eddy off Bermuda, Journal of Geophysical Research: Oceans, 104, 15 537–15 548, https://doi.org/https://doi.org/10.1029/1999JC900137, 1999.

Mcwilliams, J. C.: The vortices of two-dimensional turbulence, Journal of Fluid Mechanics, 219, 361–385, https://doi.org/10.1017/S0022112090002981, 1990.

McWilliams, J. C.: The Nature and Consequences of Oceanic Eddies, pp. 5–15, American Geophysical Union (AGU), ISBN 9781118666432, https://doi.org/https://doi.org/10.1029/177GM03, 2008.

https://doi.org/10.5194/egusphere-2026-3599
Preprint. Discussion started: 26 June 2026

Men, G., Wan, X., and Ma, W.: The Vertical Tilt of Mesoscale Eddy in the Northern South China Sea in a High-Resolution Numerical Simulation, Journal of Geophysical Research: Oceans, 129, e2024JC021 083, https://doi.org/https://doi.org/10.1029/2024JC021083, e2024JC021083 2024JC021083, 2024.

Nencioli, F., Kuwahara, V. S., Dickey, T. D., Rii, Y. M., and Bidigare, R. R.: Physical Dynamics and Biological Implications of a Mesoscale Eddy in the Lee of Hawai'i: Cyclone Opal Observations during E-Flux III, Deep Sea Research Part II: Topical Studies in Oceanography, 55, 1252–1274, https://doi.org/10.1016/j.dsr2.2008.02.003, 2008.

Nencioli, F., Dong, C., Dickey, T., Washburn, L., and McWilliams, J. C.: A Vector Geometry–Based Eddy Detection Algorithm and Its Application to a High-Resolution Numerical Model Product and High-Frequency Radar Surface Velocities in the Southern California Bight, Journal of Atmospheric and Oceanic Technology, 27, 564 – 579, https://doi.org/https://doi.org/10.1175/2009JTECHO725.1, 2010.

Okubo, A.: Horizontal dispersion of floatable particles in the vicinity of velocity singularities such as convergences, Deep Sea Research and Oceanographic Abstracts, 17, 445–454, https://doi.org/https://doi.org/10.1016/0011-7471(70)90059-8, 1970.

Payandeh, A. R., Washburn, L., Emery, B., and Ohlmann, J. C.: The Occurrence, Variability, and Potential Drivers of Submesoscale Eddies in the Southern California Bight Based on a Decade of High-Frequency Radar Observations, Journal of Geophysical Research: Oceans, 128, e2023JC019 914, https://doi.org/https://doi.org/10.1029/2023JC019914, e2023JC019914 2023JC019914, 2023.

Renault, L., Arsouze, T., and Ballabrera-Poy, J.: On the Influence of the Current Feedback to the Atmosphere on the Western Mediterranean Sea Dynamics, Journal of Geophysical Research Oceans, 126, https://doi.org/10.1029/2020jc016664, 2021.

Richardson, P.: A census of eddies observed in North Atlantic SOFAR float data, Progress in Oceanography, 31, 1–50, https://doi.org/https://doi.org/10.1016/0079-6611(93)90022-6, 1993.

Robinson, S. K.: Coherent Motions in the Turbulent Boundary Layer, Annual Review of Fluid Mechanics, 23, 601–639, https://doi.org/https://doi.org/10.1146/annurev.fl.23.010191.003125, 1991.

Rossby, T.: On the Structure and Distribution of Thin Anticyclonic Lenses in the Southeast Pacific Ocean, 72, 383–403, https://doi.org/10.1357/002224014815540651, 2014.

Rossby, T., Flagg, C., Ortner, P., and Hu, C.: A tale of two eddies: Diagnosing coherent eddies through acoustic remote sensing, Journal of Geophysical Research: Oceans, 116, https://doi.org/https://doi.org/10.1029/2011JC007307, 2011.

Roughan, M., Keating, S. R., Schaeffer, A., Cetina Heredia, P., Rocha, C., Griffin, D., Robertson, R., and Suthers, I. M.: A tale of two eddies: The biophysical characteristics of two contrasting cyclonic eddies in the East Australian Current System, Journal of Geophysical Research: Oceans, 122, 2494–2518, https://doi.org/https://doi.org/10.1002/2016JC012241, 2017.

Sadarjoen, I. A. and Post, F. H.: Detection, Quantification, and Tracking of Vortices Using Streamline Geometry, Computers & Graphics, 24, 333–341, https://doi.org/10.1016/S0097-8493(00)00029-7, 2000.

Schaeffer, A., Gramoulle, A., Roughan, M., and Mantovanelli, A.: Characterizing frontal eddies along the East Australian Current from HF radar observations, Journal of Geophysical Research: Oceans, 122, 3964–3980, https://doi.org/https://doi.org/10.1002/2016JC012171, 2017.

Veneziani, M., Griffa, A., Garraffo, Z., and Chassignet, E.: Lagrangian spin parameter and coherent structures from trajectories released in a high-resolution ocean model, Journal of Marine Research - J MAR RES, 63, https://doi.org/10.1357/0022240054663187, 2005a.

Veneziani, M., Griffa, A., Reynolds, A., Garraffo, Z., and Chassignet, E.: Parameterizations of Lagrangian spin statistics and particle dispersion in the presence of coherent vortices, Journal of Marine Research, 63, 1057–1083, https://doi.org/10.1357/002224005775247571, 2005b.

https://doi.org/10.5194/egusphere-2026-3599
Preprint. Discussion started: 26 June 2026

Vu, B. L., Stegner, A., and Arsouze, T.: Angular Momentum Eddy Detection and Tracking Algorithm (AMEDA) and Its Application to Coastal Eddy Formation, Journal of Atmospheric and Oceanic Technology, 35, 739 – 762, https://doi.org/10.1175/JTECH-D-17-0010.1, 2018.

Weiss, J.: The dynamics of enstrophy transfer in two-dimensional hydrodynamics, Physica D Nonlinear Phenomena, 48, 273–294, https://doi.org/10.1016/0167-2789(91)90088-Q, 1991.

Wiebe, E. C. and Weaver, A. J.: On the sensitivity of global warming experiments to the parametrisation of sub-grid scale ocean mixing, Climate Dynamics, 15, 875–893, https://doi.org/10.1007/s003820050319, 1999.

Yang, X., Xu, G., Liu, Y., Sun, W., Xia, C., and Dong, C.: Multi-Source Data Analysis of Mesoscale Eddies and Their Effects on Surface Chlorophyll in the Bay of Bengal, Remote Sensing, 12, https://doi.org/10.3390/rs12213485, 2020.

Zhang, Z., Tian, J., Qiu, B., Zhao, W., Chang, P., Wu, D., and Wan, X.: Observed 3D Structure, Generation, and Dissipation of Oceanic Mesoscale Eddies in the South China Sea, Scientific Reports, 6, 24 349, https://doi.org/10.1038/srep24349, 2016.